ARTICLE

https://doi.org/10.1038/s41586-019-1362-5

Single-cell analysis reveals T cell infiltration in old neurogenic niches

Ben W. Dulken[1,2,3,15], Matthew T. Buckley[1,15], Paloma Navarro Negredo[1,15], Naresha Saligrama[4,5], Romain Cayrol[6], Dena S. Leeman[1,7,12], Benson M. George[2,3], Stéphane C. Boutet[8,13], Katja Hebestreit[1,14], John V. Pluvinage[2,9], Tony Wyss-Coray[9,10], Irving L. Weissman[3], Hannes Vogel[6], Mark M. Davis[4,5,11] & Anne Brunet[1,10]*

The mammalian brain contains neurogenic niches that comprise neural stem cells and other cell types. Neurogenic niches become less functional with age, but how they change during ageing remains unclear. Here we perform single-cell RNA sequencing of young and old neurogenic niches in mice. The analysis of 14,685 single-cell transcriptomes reveals a decrease in activated neural stem cells, changes in endothelial cells and microglia, and an infiltration of T cells in old neurogenic niches. T cells in old brains are clonally expanded and are generally distinct from those in old blood, which suggests that they may experience specific antigens. T cells in old brains also express interferon-γ, and the subset of neural stem cells that has a high interferon response shows decreased proliferation in vivo. We find that T cells can inhibit the proliferation of neural stem cells in co-cultures and in vivo, in part by secreting interferon-γ. Our study reveals an interaction between T cells and neural stem cells in old brains, opening potential avenues through which to counteract age-related decline in brain function.

A hallmark of ageing is a decline in tissue function, but how changes in cell composition affect tissue function is largely unknown. The adult subventricular zone (SVZ) neurogenic niche provides a paradigm through which to address this question, as it contains different cell types—astrocytes, neural stem cells (NSCs) at different stages of commitment, endothelial cells and microglia—and it exhibits functional decline during ageing[1–16]. Age-dependent changes in this neurogenic niche have previously been documented[7–16]; however, a systematic examination at single-cell resolution of the changes that occur in this neurogenic region during ageing has not yet been performed.

Single-cell analysis of young and old neurogenic niches

Single-cell RNA-sequencing (RNA-seq) analyses have been performed on young[17–24] and old neural stem cell lineages[25,26], but a single-cell understanding of the ageing neurogenic niche is missing. To address this gap in knowledge, we performed single-cell RNA-seq of the entire SVZ in three young (3 months old) and three old (28–29 months old) mice in three independent experiments (Fig. 1a, b). Blood was removed from the mice by perfusion, and cells were rapidly dissociated from SVZ niches and subjected to fluorescence-activated cell sorting (FACS) to eliminate debris (Fig. 1a, b). Single-cell RNA-seq was performed on the entire SVZ niche using the 10x Genomics Chromium platform (Fig. 1a, b, Extended Data Fig. 1a, Supplementary Tables 1, 2). The analysis of 14,685 high-quality single-cell transcriptomes with *t*-distributed stochastic neighbour embedding (*t*-SNE) projection revealed 11 distinct cell types in the neurogenic niche (Fig. 1a). Characterization of markers in these clusters (Extended Data Fig. 1b) identified them as astrocytes and quiescent neural stem cells (astrocytes/qNSCs), activated neural stem cells and neural progenitors (aNSCs/NPCs), neuroblasts, neurons, oligodendrocyte progenitor cells, oligodendrocytes, endothelial cells, 'mural' cells (for example, pericytes), microglia, macrophages and T cells (Fig. 1a, b). Notably, the T cell population we obtained was almost exclusively from old mice (Fig. 1b, Extended Data Fig. 1c), and T cells were found to be markedly enriched in the SVZ from old mice (Fig. 1c, Supplementary Table 3). Old age was also accompanied by a decreased number of aNSCs/NPCs and neuroblasts (Fig. 1b, c, Supplementary Table 3)—as has previously been found[7–15] (although quantification of single-cell data could be influenced by differential dissociation properties with age)—as well as shifts in the transcriptomic states of microglia, endothelial cells and oligodendrocytes[26] (Fig. 1b, d, Supplementary Table 3).

Immunofluorescence staining confirmed that there was an increased number of T cells in old compared with young neurogenic regions, and that T cells were in close proximity to NSCs (Fig. 1e, f). These T cells did not co-localize with endothelial cells (Extended Data Fig. 2a), which indicates that the T cells were not in blood vessels but were within the brain parenchyma. T cell invasion in the old brain coincided with the age-dependent decline in aNSCs in the neurogenic niche (Fig. 1e, g). Therefore, T cells and NSCs could influence each other in the brains of old mice.

The analysis of our single-cell transcriptomic data revealed that T cells in old brains expressed markers of $CD8^+CD4^-$ T cells (Fig. 1h, i), and FACS experiments confirmed that old neurogenic niches were infiltrated by $CD3^+CD8^+CD4^-$ T cells (Fig. 1j, k). T cells in old brains also expressed markers of effector memory cells (low *Cd62l* and high *Cd44*), tissue retention (*Itgal* and *Itga4*) and activation (*Cd69* and *Xcl1*), including cytokines such as interferon-γ (*Ifng*)[27] (Fig. 1i). In fact, T cells were the only prominent source of interferon transcripts that we detected in this single-cell analysis (Fig. 1h, Extended Data Fig. 2b).

[1]Department of Genetics, Stanford University, Stanford, CA, USA. [2]Stanford Medical Scientist Training Program, Stanford University, Stanford, CA, USA. [3]Institute for Stem Cell Biology and Regenerative Medicine, Stanford University, Stanford, CA, USA. [4]Department of Immunology and Microbiology, Stanford University, Stanford, CA, USA. [5]Institute for Immunity, Transplantation and Infection, Stanford University School of Medicine, Stanford, CA, USA. [6]Department of Pathology, Stanford University School of Medicine, Stanford, CA, USA. [7]Cancer Biology Program, Stanford University, Stanford, CA, USA. [8]Fluidigm Corporation, South San Francisco, CA, USA. [9]Department of Neurology and Neurological Sciences, Stanford University School of Medicine, Stanford, CA, USA. [10]Glenn Laboratories for the Biology of Aging at Stanford University, Stanford University School of Medicine, Stanford, CA, USA. [11]Howard Hughes Medical Institute, Stanford University School of Medicine, Stanford, CA, USA. [12]Present address: Immunology Discovery, Genentech, South San Francisco, CA, USA. [13]Present address: 10x Genomics, Pleasanton, CA, USA. [14]Present address: Verge Genomics, South San Francisco, CA, USA. [15]These authors contributed equally: Ben W. Dulken, Matthew T. Buckley, Paloma Navarro Negredo. *e-mail: abrunet1@stanford.edu

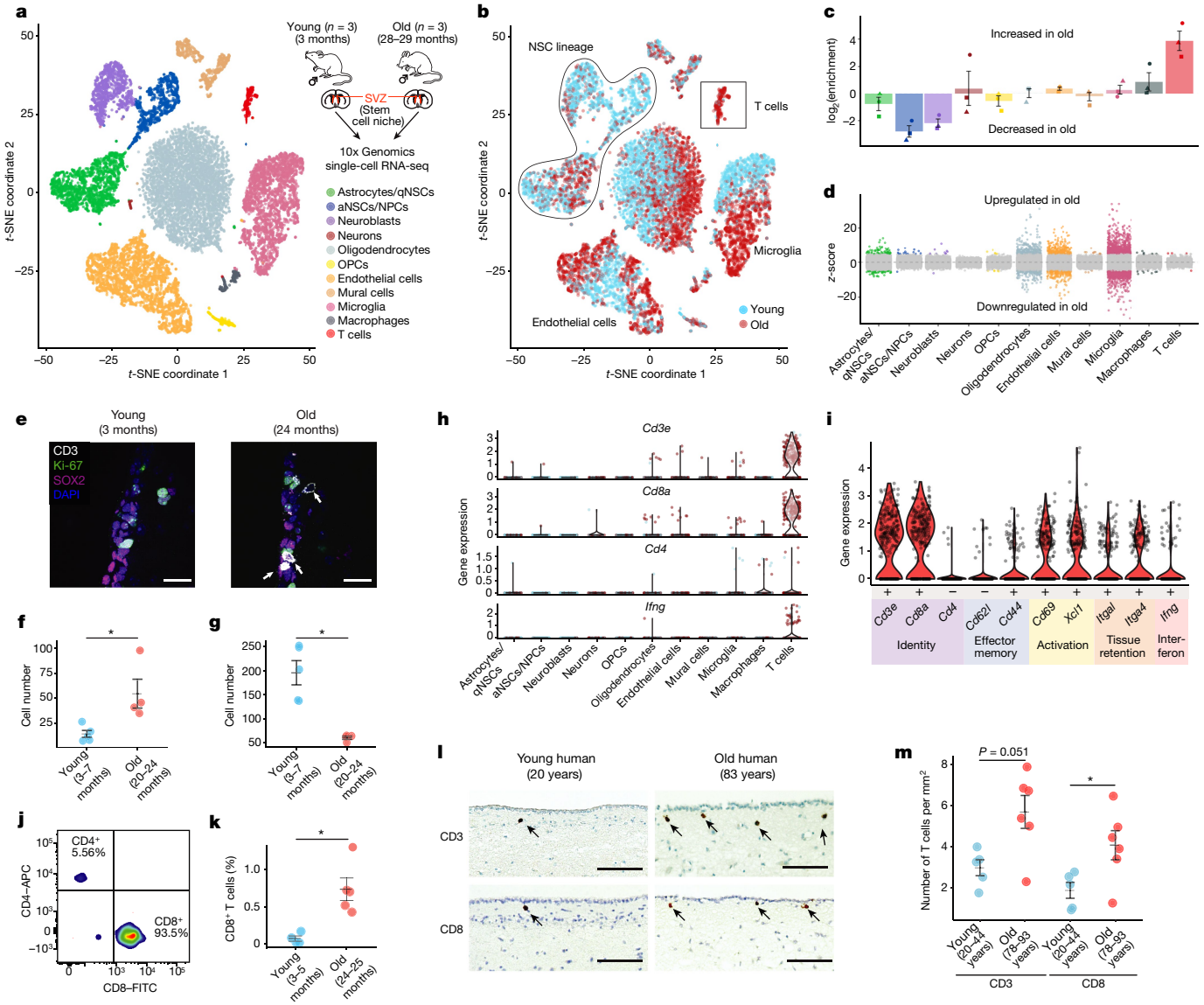

Fig. 1 | Single-cell RNA-seq reveals changes in cell composition in old neurogenic niches, with infiltration of T cells in proximity to neural stem cells. a, Single-cell RNA-seq of the SVZ from three independent replicates of young (3 months old) and old (28–29 months old) perfused male mice using the 10x Genomics Chromium platform. *t*-SNE clustering of 14,685 single-cell transcriptomes (8,884 from young and 5,801 from old) coloured by significant cell-type clusters. **b**, *t*-SNE clustering as in **a**, but coloured by age (for independent replicates, see Extended Data Fig. 1c). **c**, Age-dependent changes ($\log_2$(enrichment)) in the percentage of each cell type. Data are mean ± s.e.m. Each dot represents one replicate. **d**, Age-dependent changes in gene expression for each cell type. Each dot represents the differential expression MAST *z*-score of a gene. Dots with Bonferroni-corrected $P < 0.05$ are in colour. **e**, Immunofluorescence staining of the perfused SVZ neurogenic niche from young (3 months old) and old (24 months old) male mice. White, CD3 (T cells); magenta, SOX2 (NSCs); green, Ki-67 (cycling cells); blue, DAPI (nuclei). Scale bar, 20 μm. **f**, **g**, Number of $CD3^+$ T cells (**f**) and NSCs/NPCs ($SOX2^+Ki\text{-}67^+$) (**g**) per coronal section in five young (3–7 months old) and four old (20–24 months old) male mice. Data are mean ± s.e.m. Each dot represents cells from one mouse. $^*P = 0.020$ (**f**), $^*P = 0.016$ (**g**), two-sided Wilcoxon rank-sum test. **h**, Violin plot showing the expression of *Cd3e* (encoding CD3), *Cd8a* (encoding CD8), *Cd4* and *Ifng* in various cell types. Each dot represents the gene expression levels in one cell. $n = 6$ mice. **i**, T cells exhibit markers of effector memory T cells (low *Cd62l* and high *Cd44*), activation (*Cd69* and *Xcl1*) and tissue retention (*Itga1* and *Itga4*), and express interferon-γ (*Ifng*). Each dot represents the expression levels in one cell. $n = 6$ mice. **j**, FACS plot of T cells in the SVZ of an old (24 months old) male mouse. $CD8^+$ T cells are defined as $CD45^+CD3^+CD8^+CD4^-CD11b^-B220^-TER119^-TCR\gamma/\delta^-$. APC, allophycocyanin; FITC, fluorescein isothiocyanate. **k**, FACS quantification of the percentage of $CD8^+$ T cells per SVZ in four young (3–5 months old) and five old (24–25 months old) male mice (combined over two independent experiments, Supplementary Table 12). Data are mean ± s.e.m. Each dot represents T cells from one mouse. $^*P = 0.016$, two-sided Wilcoxon rank-sum test. **l**, Immunohistochemical staining for CD3 and CD8 (brown) in young (20 years old) and old (83 years old) human brain sections including the lateral ventricle, counterstained with haematoxylin (blue). Scale bar, 100 μm. **m**, Number of $CD3^+$ (left) or $CD8^+$ (right) T cells per unit area (mm^2) in proximity to the ventricle in five young (20–44 years old) and six old (78–93 years old) human brain sections of both sexes. Data are mean ± s.e.m. Each dot represents T cells from one human specimen (Supplementary Table 4). $^*P = 0.030$, two-sided Wilcoxon rank-sum test.

Notably, brains from elderly humans—even in the absence of neurodegenerative diseases—also exhibited infiltration of $CD8^+$ T cells in the region lining the lateral ventricle, which is a region that has neurogenic potential[16] (Fig. 1l, m, Extended Data Fig. 2c, Supplementary Table 4). We therefore conclude that the infiltration of T cells in old brains occurs in humans as well as in mice.

T cells invading old brains are clonally expanded

To characterize the T cells in old brains, we purified $CD8^+$ T cells from the neurogenic niche and the blood of the same mouse—using four different old mice in total—and performed whole-transcript single-cell RNA-seq using Smart-seq v4. T cells in the old neurogenic niche differed from those in the blood of the same old mouse (Fig. 2a, Extended

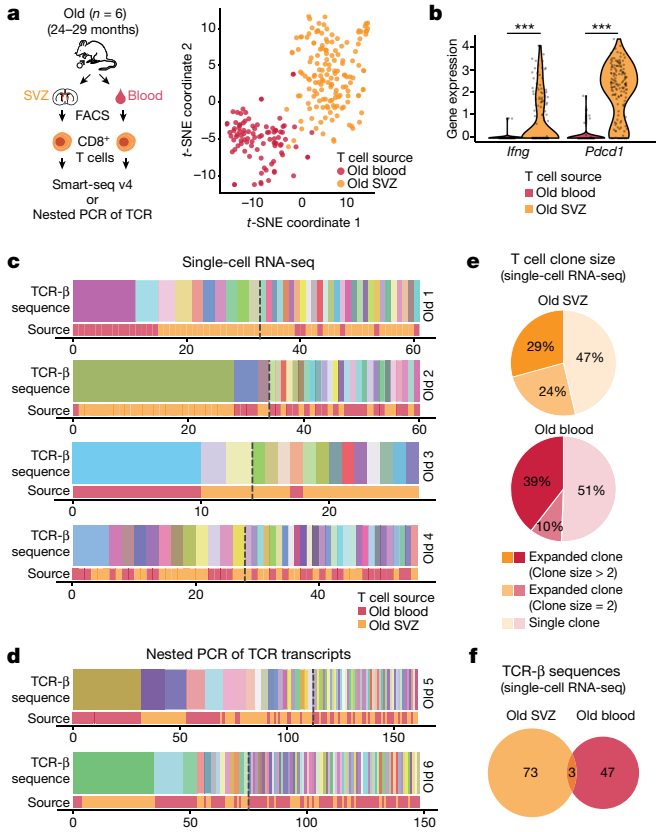

Fig. 2 | T cells invading old brains are clonally expanded and differ from T cells in old blood. a, $CD8^+$ T cells from six old (24–29 months old) male mice were isolated from the blood and perfused SVZs by FACS, and analysed by single-cell RNA-seq using Smart-seq v4 (4 mice) or nested PCR (2 mice). Left, *t*-SNE plot of 247 $CD8^+$ T cell transcriptomes, coloured by source (blood, red; SVZ, orange). Each dot represents a single T cell transcriptome ($n = 4$ old mice, 25–29 months old). **b**, Expression of *Ifng* (encoding interferon-γ) and the checkpoint gene *Pdcd1* (encoding PD-1), represented as log-normalized counts. Each dot represents expression levels in one single cell. $n = 247$ cells from four old (25–29 months old) mice. *Ifng* $^{***}P = 2.89 \times 10^{-12}$, *Pdcd1* $^{***}P = 1.29 \times 10^{-40}$; *P* values are false discovery rate (FDR)-corrected, MAST differential expression test. **c**, **d**, Clonality of T cells in the blood or in the SVZs of old mice determined by TCR sequencing from Smart-seq v4 data using TraCeR (mice 1–4) (**c**) or by nested PCR of the TCR transcripts (mice 5 and 6) (**d**). TCR-β sequence clones are ordered by decreasing frequency. The source of the T cells is indicated in the bottom row. Dashed lines indicate transitions from expanded to unique TCR-β sequence clones. **e**, Percentage of T cells isolated from the SVZ or from blood for mice 1–4 found in clones of increasing size. **f**, Venn diagram showing the lack of overlap between T cell clones from old blood and brain (SVZ) for mice 1–4. Clones were designated as clonally expanded if the same TCR β-chain sequence was detected in multiple T cells.

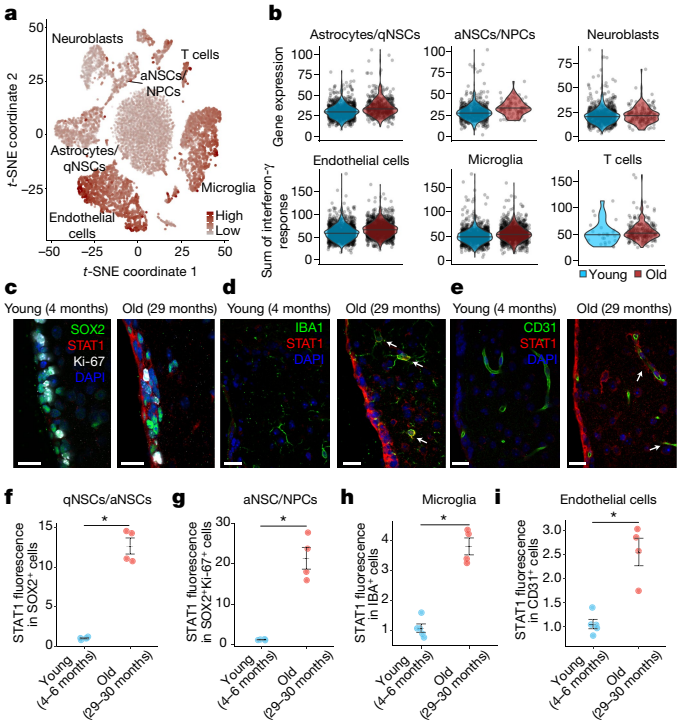

Fig. 3 | The neurogenic niche responds to interferon signalling. a, *t*-SNE plot showing combined log-normalized expression values of genes in the interferon-γ response hallmark from the Molecular Signatures Database (MSigDB) (for example, *Ifit1*, *Stat1* and *Bst2*; Supplementary Table 8) in cells of the SVZ. Darker colours indicate higher expression. $n = 14{,}685$ cells clustered as in Fig. 1a. **b**, Combined log-normalized expression values of genes in the interferon-γ response hallmark in various cell types of the SVZ. Single cells were grouped by cell type and age (Supplementary Table 3). Median cellular interferon-γ response values are denoted by horizontal lines. Astrocytes/qNSCs, $P < 2.2 \times 10^{-16}$; aNSCs/NPCs, $P = 1.4 \times 10^{-9}$; neuroblasts, $P = 0.056$, endothelial cells, $P < 2.2 \times 10^{-16}$; microglia, $P < 2.2 \times 10^{-16}$; T cells, $P = 0.230$, two-sided Wilcoxon rank-sum test. **c**–**e**, Immunofluorescence staining of STAT1 (encoded by the interferon response gene *Stat1*) in different cell types in the SVZ of young (4 months old) and old (29 months old) male mice. Red, STAT1; white, Ki-67 (cycling cells); green, SOX2 (NSCs) (**c**), IBA1 (microglia) (**d**) or CD31 (endothelial cells) (**e**); blue, DAPI (nuclei). Scale bar, 20 μm. Arrows, STAT1 staining in microglia and endothelial cells. **f**–**i**, Normalized STAT1 fluorescence intensity overlapping with cell-marker fluorescence in five young (4–6 months old) and four old (29–30 months old) male mice. Data are mean ± s.e.m. Each dot represents cells from one mouse. $^*P = 0.016$, two-sided Wilcoxon rank-sum test.

Data Fig. 3a, b, Supplementary Tables 5, 6). Unlike their counterparts from old blood, T cells from old neurogenic niches expressed high levels of interferon-γ and the immune checkpoint PD-1 (Fig. 2b, Extended Data Fig. 3c, Supplementary Tables 5, 6).

A key question is whether T cells infiltrate the old brain passively, owing to the age-related disruption of the blood–brain barrier[28], or whether they actively recognize antigens in old brains. When T cells recognize an antigen they clonally expand, with each clone expressing the same T cell receptor (TCR)[29]. To test T cell clonality, we extracted TCR sequences from single T cell transcriptomes (Fig. 2a, c). Notably, TCR analysis from four different old mice revealed that several T cells in old neurogenic niches were clonally expanded (Fig. 2c, e, f, Extended Data Fig. 3d, f, Supplementary Table 7). The TCR repertoire of old-brain T cell clones was different from that of old blood (Fig. 2c, f), which suggests that the T cells in old brains did not simply originate from passive diffusion through a disrupted blood–brain barrier with ageing. We confirmed these differences using nested PCR (Fig. 2d, Extended Data Fig. 3e, g, h, Supplementary Table 7). Thus, T cells in old brains are clonally expanded and differ from those in old blood in that they express different TCRs and exhibit high levels of interferon-γ transcripts.

The neurogenic niche responds to interferon signalling

Interferons are important for defence against pathogens[30] and abnormal endogenous nucleotides[31,32]. The effect of interferons has been examined in the developing brain and adult neurogenic niche[26,33–36], but the role of interferon-γ remains unclear. Analysis of our single-cell data revealed that several cell types in the neurogenic niche (astrocytes/qNSCs, aNSCs/NPCs, endothelial cells and microglia) expressed the interferon-γ receptor (Extended Data Fig. 4a, b) and exhibited an age-associated increase in the interferon-γ response signature (for example, expression of *Ifit1*, *Stat1* and *Bst2*, Supplementary Table 8) (Fig. 3a, b, Extended Data Fig. 4c, d, g–j). Immunofluorescence

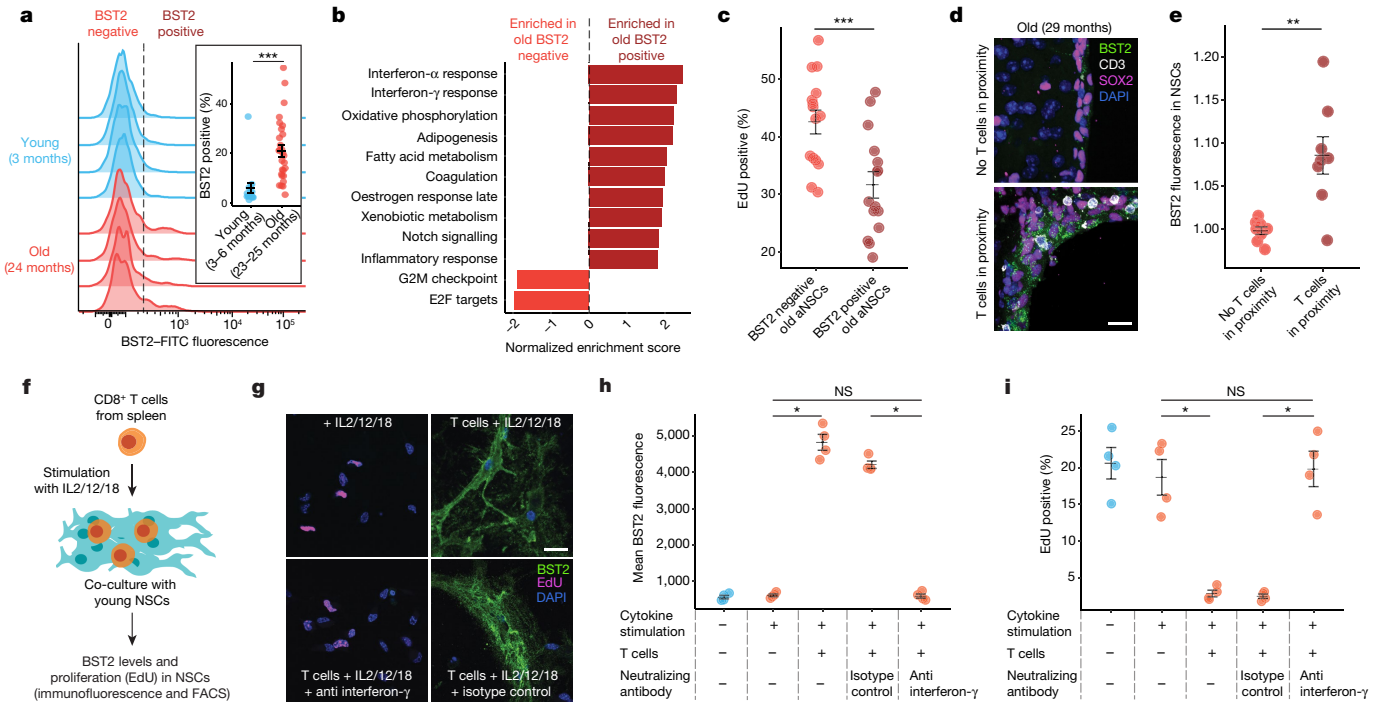

Fig. 4 | Interferon-γ signalling from T cells negatively affects NSCs. **a**, FACS histograms of BST2 fluorescence in aNSCs/NPCs from young (3 months old, $n = 4$) and old (24 months old, $n = 4$) mice. The inset shows the percentage of aNSCs/NPCs that are BST2-positive out of the approximately 500 cells analysed from each young ($n = 15$, 3–6 months old) or old ($n = 28$, 23–25 months old) mouse (combined over 5 experiments, Supplementary Table 12). Data are mean ± s.e.m. $***P = 1.10 \times 10^{-5}$, two-sided Wilcoxon rank-sum test. **b**, Hallmark gene set enrichment analysis (GSEA) of bulk RNA-seq data from freshly isolated BST2-positive compared with BST2-negative aNSCs/NPCs from old mice (24 months old, $n = 4$). For all pathways shown, FDR < 0.01, GSEA statistics. **c**, FACS quantification of the percentage of cells that are EdU-positive (4 h after EdU injection) out of the approximately 100 BST2-positive and BST2-negative aNSCs/NPCs isolated from old male mice ($n = 15$, 23–25 months old) (combined over 3 experiments, Supplementary Table 12). Data are mean ± s.e.m. Each dot represents cells from one mouse. $***P = 3.23 \times 10^{-4}$, two-sided Wilcoxon rank-sum test. **d**, Immunofluorescence staining of SVZ sections from an old (29 months old) male mouse. White, CD3 (T cells); magenta, SOX2 (NSCs); green, BST2 (interferon response); blue, DAPI (nuclei). Scale bar, 20 μm. **e**, Quantification of BST2 fluorescence in NSCs in proximity (or not) to $CD3^+$ T cells in SVZ sections from three old (29–30 months old) mice. Data represent mean ± s.e.m. Each dot represents normalized BST2 fluorescence in $SOX2^+$ NSCs in one section. $**P = 0.007$, two-sided Wilcoxon rank-sum test. **f**, Scheme for the co-culture of T cells and NSCs. **g**, Immunofluorescence staining of cultured NSCs from young mice (3 months old) co-cultured with T cells and cytokines with or without the addition of a neutralizing antibody to interferon-γ. Green, BST2 (high interferon response); red, EdU (proliferating cells); blue, DAPI (nuclei). Scale bar, 20 μm. **h**, **i**, FACS quantification of the percentage of NSCs that are BST2-positive (**h**) or EdU-positive after a 4-h EdU pulse (**i**) of the approximately 1,000 cells analysed from each NSC culture co-cultured with splenic $CD8^+$ T cells with or without addition of a neutralizing antibody to interferon-γ. $n = 4$ for each condition. Representative of two independent experiments (see Supplementary Table 12). Data are mean ± s.e.m. Each dot represents the mean fluorescence of an NSC culture derived from one mouse. $*P = 0.029$, two-sided Wilcoxon rank-sum test. NS, not significant.

staining and FACS analysis revealed strongly increased staining of STAT1—a protein that is upregulated upon interferon signalling[33]—in old aNSCs/NPCs, microglia and endothelial cells compared with their younger counterparts (Fig. 3c–i, Extended Data Fig. 4e, f). Therefore, multiple cell types in the old neurogenic niche—including NSCs—experience a strong response to interferon-γ, although they may also be responding to other interferons[26].

Interferon-γ from T cells negatively affects NSCs

We characterized the response of NSCs to interferon-γ. Principal component analysis using only genes associated with the interferon-γ response revealed that a subpopulation of old astrocytes/qNSCs and aNSCs/NPCs experience a high interferon-γ response (Extended Data Fig. 5a–c, Supplementary Table 9). FACS analysis confirmed that only a subpopulation of old qNSCs and aNSC/NPCs showed increased STAT1 staining (Extended Data Fig. 5d). Old NSCs therefore exhibit a heterogeneous interferon-γ response.

We next determined whether the subpopulation of old NSCs that experiences a strong interferon-γ response differs from its non-responsive counterpart. To isolate this subpopulation, we searched for a surface marker that correlated with the interferon-γ response. We identified BST2 (encoded by *Bst2*; also known as tetherin in humans), a surface protein that is involved in viral vesicle budding in response to interferons[37–39] (Extended Data Fig. 5e). FACS analysis confirmed that a subpopulation of aNSCs/NPCs from old mice showed increased BST2 expression (Fig. 4a, Extended Data Fig. 5f, g). Bulk RNA-seq analysis validated that the BST2-positive subpopulation of old aNSCs/NPCs was strongly enriched for genes that are associated with the interferon-γ response, compared to its BST2-negative counterpart (Fig. 4b, Supplementary Tables 10, 11). The subpopulation of BST2-positive aNSCs/NPCs from old mice was depleted in transcripts that are related to the cell cycle, compared to its BST2-negative counterpart (Fig. 4b). To assess the proliferation status of the subset of old NSCs that experience a high interferon-γ response, we injected old mice with 5-ethynyl-2′-deoxyuridine (EdU), which incorporates in proliferating cells. The BST2-positive subpopulation of old aNSCs/NPCs exhibited reduced EdU incorporation and decreased staining for Ki-67 (another marker of cycling cells) compared to its BST2-negative counterpart (Fig. 4c, Extended Data Fig. 5h). Thus, the subset of old NSCs that exhibits a strong interferon-γ response is dysfunctional in vivo.

We next asked whether T cells could contribute to the high interferon response in NSCs and affect their proliferation. The presence of T cells in the neurogenic niche was correlated with an increase in BST2 in the

NSCs that are in close proximity to these T cells (Fig. 4d, e). We found that forcing the entry of $CD8^+$ T cells into the brains of young mice—by injecting the brain-specific antigen myelin oligodendrocyte glycoprotein (MOG)[40,41] (Extended Data Fig. 6a–c)—was associated with an increase in BST2-positive aNSCs/NPCs, which exhibited reduced proliferation in vivo (Extended Data Fig. 6d, e). Although MOG also induces other immune responses[40,41], these results suggest that T cells impair NSC proliferation in vivo.

To test whether T cells can directly affect the proliferation of NSCs, we co-cultured $CD8^+$ T cells with NSCs that had been isolated from young mice (Fig. 4f). Immunofluorescence and FACS analyses both indicated that the addition of T cells, in the presence of a cytokine cocktail that promotes the production of interferon-γ in T cells[42], induced BST2 expression in NSCs (Fig. 4g, h) and markedly reduced NSC proliferation (Fig. 4g, i). Both the induction of BST2 and the reduction in NSC proliferation in the presence of activated T cells were reversed by the addition of an antibody that neutralizes interferon-γ (Fig. 4g–i). Similar effects were observed when T cells were activated using antibodies to CD3 and CD28 (Extended Data Fig. 6f, g). T cells can therefore directly inhibit NSC proliferation by the secretion of interferon-γ. However, other cells—such as microglia or endothelial cells—could also contribute to NSC dysfunction in vivo.

Discussion

Our study provides a systems-level understanding of the old neurogenic niche in the mammalian brain and shows that T cells infiltrate this niche with age. Notably, these T cells are clonally expanded and differ from blood T cells, which suggests that they may recognize a specific antigen in the old brain. T cells were recently shown to infiltrate the brain in the context of neurodegenerative diseases[43–45] and during ageing[46,47]. However, their clonal expansion in the old neurogenic niche had not been reported. T cells that infiltrate into old neurogenic niches might recognize neoantigens, including those from aggregated proteins in old NSCs[14]. Other cells in the old neurogenic niche—such as microglia[48], endothelial cells[49] or other immune cells in the brain such as macrophages[47]—could provide chemokines to attract T cells.

Although T cells can influence the nervous system during development and youth[36,50–52] and during disease (for example, during infection[53,54] or in multiple sclerosis[40,41]), their role during ageing is not clear. We show that brain T cells express interferon-γ, and that several cells in the niche—including NSCs—exhibit an interferon-γ response. The interferon-γ response that is induced by T cells appears to be detrimental for NSC function in vitro and in vivo. Although the exact link between T cells, interferon and NSC proliferation remains to be established, our results provide a possible cause for the decline of NSC during ageing and suggest avenues through which to counteract age-associated cognitive impairment.

Online content

Any methods, additional references, Nature Research reporting summaries, source data, statements of data availability and associated accession codes are available at https://doi.org/10.1038/s41586-019-1362-5.

Received: 6 June 2018; Accepted: 4 June 2019;
Published online 3 July 2019.

1. Mirzadeh, Z., Merkle, F. T., Soriano-Navarro, M., Garcia-Verdugo, J. M. & Alvarez-Buylla, A. Neural stem cells confer unique pinwheel architecture to the ventricular surface in neurogenic regions of the adult brain. *Cell Stem Cell* **3**, 265–278 (2008).
2. Shen, Q. et al. Adult SVZ stem cells lie in a vascular niche: a quantitative analysis of niche cell-cell interactions. *Cell Stem Cell* **3**, 289–300 (2008).
3. Tavazoie, M. et al. A specialized vascular niche for adult neural stem cells. *Cell Stem Cell* **3**, 279–288 (2008).
4. Codega, P. et al. Prospective identification and purification of quiescent adult neural stem cells from their in vivo niche. *Neuron* **82**, 545–559 (2014).
5. Bond, A. M., Ming, G. L. & Song, H. Adult mammalian neural stem cells and neurogenesis: five decades later. *Cell Stem Cell* **17**, 385–395 (2015).
6. Gage, F. H. & Temple, S. Neural stem cells: generating and regenerating the brain. *Neuron* **80**, 588–601 (2013).
7. Maslov, A. Y., Barone, T. A., Plunkett, R. J. & Pruitt, S. C. Neural stem cell detection, characterization, and age-related changes in the subventricular zone of mice. *J. Neurosci.* **24**, 1726–1733 (2004).
8. Luo, J., Daniels, S. B., Lennington, J. B., Notti, R. Q. & Conover, J. C. The aging neurogenic subventricular zone. *Aging Cell* **5**, 139–152 (2006).
9. Chaker, Z., Aïd, S., Berry, H. & Holzenberger, M. Suppression of IGF-I signals in neural stem cells enhances neurogenesis and olfactory function during aging. *Aging Cell* **14**, 847–856 (2015).
10. Enwere, E. et al. Aging results in reduced epidermal growth factor receptor signaling, diminished olfactory neurogenesis, and deficits in fine olfactory discrimination. *J. Neurosci.* **24**, 8354–8365 (2004).
11. Tropepe, V., Craig, C. G., Morshead, C. M. & van der Kooy, D. Transforming growth factor-α null and senescent mice show decreased neural progenitor cell proliferation in the forebrain subependyma. *J. Neurosci.* **17**, 7850–7859 (1997).
12. Molofsky, A. V. et al. Increasing p16INK4a expression decreases forebrain progenitors and neurogenesis during ageing. *Nature* **443**, 448–452 (2006).
13. Ahlenius, H., Visan, V., Kokaia, M., Lindvall, O. & Kokaia, Z. Neural stem and progenitor cells retain their potential for proliferation and differentiation into functional neurons despite lower number in aged brain. *J. Neurosci.* **29**, 4408–4419 (2009).
14. Leeman, D. S. et al. Lysosome activation clears aggregates and enhances quiescent neural stem cell activation during aging. *Science* **359**, 1277–1283 (2018).
15. Silva-Vargas, V., Maldonado-Soto, A. R., Mizrak, D., Codega, P. & Doetsch, F. Age-dependent niche signals from the choroid plexus regulate adult neural stem cells. *Cell Stem Cell* **19**, 643–652 (2016).
16. Ernst, A. et al. Neurogenesis in the striatum of the adult human brain. *Cell* **156**, 1072–1083 (2014).
17. Llorens-Bobadilla, E. et al. Single-cell transcriptomics reveals a population of dormant neural stem cells that become activated upon brain injury. *Cell Stem Cell* **17**, 329–340 (2015).
18. Hochgerner, H. Z., Amit, A., Lönnerberg, P. & Linnarsson, S. Conserved properties of dentate gyrus neurogenesis across postnatal development revealed by single-cell RNA sequencing. *Nat. Neurosci.* **21**, 290–299 (2018).
19. Shin, J. et al. Single-cell RNA-seq with waterfall reveals molecular cascades underlying adult neurogenesis. *Cell Stem Cell* **17**, 360–372 (2015).
20. Dulken, B. W., Leeman, D. S., Boutet, S. C., Hebestreit, K. & Brunet, A. Single-cell transcriptomic analysis defines heterogeneity and transcriptional dynamics in the adult neural stem cell lineage. *Cell Rep.* **18**, 777–790 (2017).
21. Luo, Y. et al. Single-cell transcriptome analyses reveal signals to activate dormant neural stem cells. *Cell* **161**, 1175–1186 (2015).
22. Mizrak, D. et al. Single-cell analysis of regional differences in adult V-SVZ neural stem cell lineages. *Cell Rep.* **26**, 394–406.e5 (2019).
23. Zywitza, V., Misios, A., Bunatyan, L., Willnow, T. E. & Rajewsky, N. Single-cell transcriptomics characterizes cell types in the subventricular zone and uncovers molecular defects impairing adult neurogenesis. *Cell Rep.* **25**, 2457–2469.e8 (2018).
24. Basak, O. et al. $Troy^+$ brain stem cells cycle through quiescence and regulate their number by sensing niche occupancy. *Proc. Natl Acad. Sci. USA* **115**, E610–E619 (2018).
25. Shi, Z. et al. Single-cell transcriptomics reveals gene signatures and alterations associated with aging in distinct neural stem/progenitor cell subpopulations. *Protein Cell* **9**, 351–364 (2018).
26. Kalamakis, G. et al. Quiescence modulates stem cell maintenance and regenerative capacity in the aging brain. *Cell* **176**, 1407–1419.e14 (2019).
27. Haring, J. S., Badovinac, V. P. & Harty, J. T. Inflaming the $CD8^+$ T cell response. *Immunity* **25**, 19–29 (2006).
28. Montagne, A. et al. Blood-brain barrier breakdown in the aging human hippocampus. *Neuron* **85**, 296–302 (2015).
29. Han, A., Glanville, J., Hansmann, L. & Davis, M. M. Linking T-cell receptor sequence to functional phenotype at the single-cell level. *Nat. Biotechnol.* **32**, 684–692 (2014).
30. Schroder, K., Hertzog, P. J., Ravasi, T. & Hume, D. A. Interferon-gamma: an overview of signals, mechanisms and functions. *J. Leukoc. Biol.* **75**, 163–189 (2004).
31. Yu, Q. et al. Type I interferon controls propagation of long interspersed element-1. *J. Biol. Chem.* **290**, 10191–10199 (2015).
32. De Cecco, M. et al. L1 drives IFN in senescent cells and promotes age-associated inflammation. *Nature* **566**, 73–78 (2019).
33. Pereira, L., Medina, R., Baena, M., Planas, A. M. & Pozas, E. IFN gamma regulates proliferation and neuronal differentiation by STAT1 in adult SVZ niche. *Front. Cell. Neurosci.* **9**, 270 (2015).
34. Baruch, K. et al. Aging-induced type I interferon response at the choroid plexus negatively affects brain function. *Science* **346**, 89–93 (2014).
35. Li, L., Walker, T. L., Zhang, Y., Mackay, E. W. & Bartlett, P. F. Endogenous interferon gamma directly regulates neural precursors in the non-inflammatory brain. *J. Neurosci.* **30**, 9038–9050 (2010).
36. Filiano, A. J. et al. Unexpected role of interferon-γ in regulating neuronal connectivity and social behaviour. *Nature* **535**, 425–429 (2016).
37. Yoo, H., Park, S. H., Ye, S. K. & Kim, M. IFN-γ-induced BST2 mediates monocyte adhesion to human endothelial cells. *Cell. Immunol.* **267**, 23–29 (2011).
38. Holmgren, A. M., Miller, K. D., Cavanaugh, S. E. & Rall, G. F. Bst2/tetherin is induced in neurons by type I interferon and viral infection but is dispensable for protection against neurotropic viral challenge. *J. Virol.* **89**, 11011–11018 (2015).
39. Evans, D. T., Serra-Moreno, R., Singh, R. K. & Guatelli, J. C. BST-2/tetherin: a new component of the innate immune response to enveloped viruses. *Trends Microbiol.* **18**, 388–396 (2010).

40. Constantinescu, C. S., Farooqi, N., O'Brien, K. & Gran, B. Experimental autoimmune encephalomyelitis (EAE) as a model for multiple sclerosis (MS). *Br. J. Pharmacol.* **164**, 1079–1106 (2011).
41. Weiss, H. A., Millward, J. M. & Owens, T. $CD8^+$ T cells in inflammatory demyelinating disease. *J. Neuroimmunol.* **191**, 79–85 (2007).
42. Raué, H. P., Brien, J. D., Hammarlund, E. & Slifka, M. K. Activation of virus-specific $CD8^+$ T cells by lipopolysaccharide-induced IL-12 and IL-18. *J. Immunol.* **173**, 6873–6881 (2004).
43. Town, T., Tan, J., Flavell, R. A. & Mullan, M. T-cells in Alzheimer's disease. *Neuromolecular Med.* **7**, 255–264 (2005).
44. Sulzer, D. et al. T cells from patients with Parkinson's disease recognize α-synuclein peptides. *Nature* **546**, 656–661 (2017).
45. Buckwalter, M. S. et al. Increased T cell recruitment to the CNS after amyloid β_{1-42} immunization in Alzheimer's mice overproducing transforming growth factor-β1. *J. Neurosci.* **26**, 11437–11441 (2006).
46. Ritzel, R. M. et al. Age-associated resident memory CD8 T cells in the central nervous system are primed to potentiate inflammation after ischemic brain injury. *J. Immunol.* **196**, 3318–3330 (2016).
47. Mrdjen, D. et al. High-dimensional single-cell mapping of central nervous system immune cells reveals distinct myeloid subsets in health, aging, and disease. *Immunity* **48**, 380–395.e6 (2018).
48. Salter, M. W. & Stevens, B. Microglia emerge as central players in brain disease. *Nat. Med.* **23**, 1018–1027 (2017).
49. Pober, J. S. & Sessa, W. C. Evolving functions of endothelial cells in inflammation. *Nat. Rev. Immunol.* **7**, 803–815 (2007).
50. Kokaia, Z., Martino, G., Schwartz, M. & Lindvall, O. Cross-talk between neural stem cells and immune cells: the key to better brain repair? *Nat. Neurosci.* **15**, 1078–1087 (2012).
51. Louveau, A., Harris, T. H. & Kipnis, J. Revisiting the mechanisms of CNS immune privilege. *Trends Immunol.* **36**, 569–577 (2015).
52. Ziv, Y., Avidan, H., Pluchino, S., Martino, G. & Schwartz, M. Synergy between immune cells and adult neural stem/progenitor cells promotes functional recovery from spinal cord injury. *Proc. Natl Acad. Sci. USA* **103**, 13174–13179 (2006).
53. McGavern, D. B., Homann, D. & Oldstone, M. B. A. T cells in the central nervous system: the delicate balance between viral clearance and disease. *J. Infect. Dis.* **186** (Suppl 2), S145–S151 (2002).
54. Wakim, L. M., Woodward-Davis, A. & Bevan, M. J. Memory T cells persisting within the brain after local infection show functional adaptations to their tissue of residence. *Proc. Natl Acad. Sci. USA* **107**, 17872–17879 (2010).

Acknowledgements We thank D. Wagh from the Stanford Functional Genomics Facility for assistance with 10x Genomics libraries and Fluidigm Corporation for help with Fluidigm C1 libraries; the Stanford Shared FACS Facility and C. Carswell-Crumpton for FACS support; and T. Palmer, T. Rando, A. Kundaje, M. Monje-Deisseroth and V. Sebastiano for guidance. This work was supported by NIH P01 AG036695 (A.B.), a generous gift from T. and M. Barakett (A.B.), NIH T32 GM7365 (B.W.D.), the Stanford MSTP program (B.W.D.), an NSF Graduate Research Fellowship (M.T.B.), a Human Frontiers Science Program Long-term Fellowship (P.N.N.), and a Postdoctoral Fellowship and Career Transition Grant from the National Multiple Sclerosis Society (N.S.).

Reviewer information *Nature* thanks Burkhard Ludewig, Hongjun Song and the other anonymous reviewer(s) for their contribution to the peer review of this work.

Author contributions B.W.D. and A.B. planned the study. B.W.D. performed and analysed most experiments, except for those indicated below. M.T.B. performed one 10x Genomics and Smart-seq v4 replicate and analysed the combined data. P.N.N. designed and analysed human brain experiments and performed and analysed immunocytochemistry in vivo and in culture. N.S. performed TCR sequencing by nested PCR and MOG injection under the supervision of M.M.D. R.C. and H.V. provided human brain tissues and helped with design. S.C.B. helped with Fluidigm C1 libraries. D.S.L. helped with the NSC FACS protocol. K.H. helped with statistical analysis. B.M.G., J.V.P., T.W.-C., I.L.W. and M.M.D. provided intellectual contribution. B.W.D. and A.B. wrote the initial manuscript, and M.T.B. and P.N.N. wrote the revised version.

Competing interests The authors declare no competing interests.

Additional information
Extended data is available for this paper at https://doi.org/10.1038/s41586-019-1362-5.
Supplementary information is available for this paper at https://doi.org/10.1038/s41586-019-1362-5.
Reprints and permissions information is available at http://www.nature.com/reprints.
Correspondence and requests for materials should be addressed to A.B.
Publisher's note: Springer Nature remains neutral with regard to jurisdictional claims in published maps and institutional affiliations.

METHODS

Data reporting. No statistical methods were used to predetermine sample size. The experiments were not randomized, and the investigators were not blinded to allocation during experiments and outcome assessment except when using human samples.

Laboratory animals. All mice used in this study were male C57BL/6 mice. For experiments using paired young and old mice, or old mice alone, mice were obtained from the NIA Aged Rodent colony. For experiments performed exclusively in young mice, mice were obtained from the Jackson Laboratory. Mice were habituated for more than one week at Stanford before use. At Stanford, all mice were housed in the Comparative Medicine Pavilion or the Research Animal Facility II, and their care was monitored by the Veterinary Service Center at Stanford University under IUCAC protocols 8661 and 28396.

Single-cell RNA-seq from young and old SVZ using 10x Genomics Chromium. We performed single-cell RNA-seq of all live cells in the SVZ neurogenic niche. To this end, we used three young (3 months old), and three old (28–29 months old) male C57BL/6 mice from the NIA aged colony in three independent experiments, performed by two independent investigators (B.W.D. performed the first two experiments, and M.T.B. performed the third experiment). Specifically, mice were sedated and perfused with 20 ml of PBS with heparin sodium salt (50 U ml^{-1}) (Sigma-Aldrich) to remove the blood, and brains were immediately collected. As previously described[4], the SVZ from each hemisphere was micro-dissected and dissociated with enzymatic digestion with papain for 10 min at a concentration of 14 U ml^{-1}. The dissociated SVZ was then triturated in a solution containing 0.7 mg ml^{-1} ovomucoid and 0.5 mg ml^{-1} DNaseI in DMEM/F12. The dissociated cells from the SVZ were then centrifuged through 22% Percoll in PBS to remove myelin debris. After centrifugation through Percoll solution, cells were washed with FACS buffer (HBSS, 1% BSA, 0.1% glucose). Live/dead staining was performed using 1 μg ml^{-1} propidium iodide (BioLegend). FACS sorting was performed on a BD FACS Aria II sorter, using a 100-μm nozzle at 13.1 PSI. Cells were sorted into catching medium: DMEM/F12 (Thermo Fisher) with B27 supplement (Thermo Fisher, no Vitamin A, 1:50), N2 supplement (Thermo Fisher, 1:100), 15 mM HEPES buffer, 0.6% glucose, penicillin–streptomycin–glutamine (Life Technologies, 1:100), and insulin–transferrin–selenium (Life Technologies, 1:1,000). Cells were then spun down at 300*g* for 5 min at 4 °C and resuspended in catching medium at a concentration of 300 cells per μl.

Cells were loaded onto a 10x Genomics Chromium chip per factory recommendations. Reverse transcription and library preparation was performed using the 10x Genomics Single Cell v2 kit following the 10x Genomics protocol. One young and one old library were multiplexed and sequenced on one lane of Illumina NextSeq-500 with a high output (400m) kit.

Quality control of 10x Genomics single-cell RNA-seq. For mapping, sequences obtained from sequencing using the 10x Genomics single-cell RNA-seq platform were demultiplexed and mapped to the mm10 transcriptome using the Cell Ranger package (10x Genomics). Cells were removed if they expressed fewer than 400 unique genes, more than 4,500 unique genes or greater than 15% mitochondrial reads. Genes not detected in any cell were removed from subsequent analysis. The levels of mitochondrial reads and numbers of unique molecular identifiers (UMIs) were similar between the young and old conditions (Supplementary Table 2), which indicates that there were no systematic biases in the libraries from young and old mice. The average gene detection in each cell type was similar between young and old (Extended Data Fig. 1a). Our study includes 14,685 cells, with 8,884 cells from young (young 1, 2,306; young 2, 2,675; young 3, 3,903) and 5,801 cells from old (old 1, 1,435; old 2, 2,541; old 3, 1,825).

***t*-SNE analysis of single-cell RNA-seq datasets and identification of cell clusters.** To analyse the single-cell RNA-seq data, we performed *t*-SNE clustering using the Seurat R Package (v. 2.3.4) with the first 15 principal components[55], after performing principal component analysis (PCA) on the 4,125 most variable genes. Identification of significant clusters was performed using the FindClusters() algorithm in the Seurat package which uses a shared nearest neighbour modularity optimization-based clustering algorithm[55]. Marker genes for each significant cluster were found using the Seurat function FindAllMarkers(). Cell types were determined using a combination of marker genes identified from the literature and gene ontology for cell types using the web-based tool Enrichr (http://amp.pharm.mssm.edu/Enrichr/). This analysis identified 11 clusters of cells: astrocytes/qNSCs, aNSCs/NPCs, neuroblasts, neurons, oligodendrocyte progenitor cells, oligodendrocytes, endothelial cells, 'mural' cells (for example, pericytes or smooth muscle), microglia, macrophages and T cells. We note that ependymal cells—a known component of the NSC niche[56,57]—were not identified, probably because these cells were too big to be uploaded in droplets, or were sheared in the 10x microfluidic device. In addition, we note that the quantification of single-cell data could be also influenced by different dissociation properties with age.

Clustering, heat maps and violin plots for gene expression in single cells. Hierarchical clustering and heat-map generation were performed for single cells on the basis of log-normalized (with scale factor 10,000 and pseudocount 1) expression values of marker genes curated from literature or identified as highly differentially expressed. Heat maps were generated using the heatmap.2 function from the gplots v3.0.1 R package using the default complete-linkage clustering algorithm. To visualize the expression of individual genes, cells were grouped by their cell type as determined by analysis with Seurat. log-normalized gene expression values were plotted for each cell as a violin plot with an overlying dot plot in R.

Immunostaining of brain sections. All immunostainings were performed on C57BL/6 mice obtained from the NIA at the age indicated. Mice were subjected to intracardiac perfusion with 5 ml of PBS containing heparin followed by 20 ml of 4% paraformaldehyde in PBS. Brains were post-fixed for 24 h in 4% paraformaldehyde. They were then subjected to dehydration in 30% sucrose. Brains were subsequently embedded in optimal cutting temperature compound and sectioned in 12-μm coronal sections that were mounted on glass slides. To perform immunofluorescent staining, sections were first washed with PBS, followed by permeabilization in ice-cold methanol with 0.2% Triton-X for 10 min at room temperature. Sections were blocked with 5% normal donkey serum (ImmunoReagents) and 1% BSA (Fisher Biosciences) in PBS for 30 min at room temperature. Primary antibody staining was performed overnight at 4 °C in 5% normal donkey serum and 1% BSA in PBS. Primary antibodies used were the following: BST2 (BioLegend, Clone: 927, lot: B256699, (1:200)), CD3 (Novus Biological, Clone: SP7, lot: L139 and J275, (1:200)), CD31 (R&D Systems, product no.:AF3628, lot: YZU0117021, (1:500)), IBA1 (Novus Biological, product no.: NB100-1028, lot: S7C7G2P24-E250517, (1:500)), Ki-67 (eBioscience, Clone: SolA15, lot: 4328926, (1:500)), SOX2 (R&D Systems, product no.: AF2018, KOY0317071, (1:200)), STAT1 (Cell Signaling, Clone: D1K9Y, lot: 4 (1:500)). Sections were washed with PBS with 0.2% Tween and then with PBS only 3 times for 5 min at room temperature. Secondary antibody staining was performed at room temperature for 2 h in 5% normal donkey serum and 1% BSA in PBS. Secondary antibodies used were the following: donkey anti rabbit-AF568 (Thermo Fisher (1:500)), donkey anti rat-AF488 (Thermo Fisher (1:500)) and donkey anti goat-AF647 (Thermo Fisher (1:500)). Sections were washed with 0.2% Tween and then with PBS 3 times for 5 min at room temperature. Sections were stained with DAPI at 1 μg ml^{-1} for 10 min at room temperature. Sections were mounted with ProLong Gold (Thermo Fisher) and visualized with a Nikon Eclipse Ti confocal microscope equipped with a Zyla sCMOS camera (Andor) and NIS-Elements software (AR 4.30.02, 64-bit) using the 20×, 60× or 100× objective. No blinding was performed for taking pictures. For visualization of images displayed in this manuscript, brightness and contrast were adjusted in Fiji to enhance visualization (these adjustments were not performed before the quantification described below). The same settings were applied to all images shown for each experiment.

Confocal microscopy image analysis and quantification. *T cell and NSC quantification.* The number of $CD3^+$ T cells was manually counted in entire coronal sections of five young (3–7 months old) and four old (20–24 months old) male mice while directly visualizing each section under the microscope with the 20× objective. T cells were identified as $CD3^+DAPI^+$. Note that we observed the presence of T cells in various regions of old brains, not just the SVZ. The number of proliferative NSCs/NPCs ($SOX2^+Ki\text{-}67^+$) in the same sections and mice was counted manually while directly visualizing each section under the microscope with the 20× objective. NSCs/NPCs were identified as $SOX2^+Ki\text{-}67^+DAPI^+$. The mean number of T cells or NSCs per coronal section was calculated for four sections in total per mouse. The mean ± s.e.m. was plotted and was used for the calculation of *P* values using the Wilcoxon rank-sum test.

STAT1 quantification. The entire SVZ area in both brain hemispheres was imaged using the 60× objective. Images were collected from five young (4–6 months old) and four old (29–30 months old) wild-type C57BL/6 male mice. Two brain sections were imaged per mouse. Fiji (ImageJ) was used for image analysis. Channels were split and image backgrounds were subtracted using a rolling ball radius chosen on the basis of the size of the object being analysed. A 50-pixel rolling ball radius was used for STAT1 and 100-pixel rolling ball radius was used for Ki-67 (a marker of cycling cells), SOX2 (a marker of the NSC lineage), IBA1 (a marker of microglia) and CD31 (a marker of endothelial cells). The same settings were applied to all experimental conditions. In SVZ sections from old mice, STAT1 co-localized with SOX2 (NSC lineage), IBA1 (microglia) and CD31 (endothelial cells). There was also co-localization between STAT1 and another NSC marker, glial fibrillary acidic protein (GFAP). The STAT1 fluorescence co-localizing with the cell marker of interest was quantified using a custom pipeline. In brief, the channel for the cell type of interest (NSCs, microglia or endothelial) was used to generate a mask by setting intensity thresholds to outline the positive areas. The same threshold values were used for all images across all conditions in each individual experiment. The cell masks were then used to determine the STAT1 fluorescence levels by mean intensity per masked pixel. The mean intensity STAT1 values were normalized for each independent experiment by dividing them by the median intensity of the young samples and the mean of these normalized values was used for plotting and calculating *P* values using the Wilcoxon rank-sum test.

BST2 quantification in NSCs that are in proximity to T cells. *Z*-stacks of the entire SVZ area in both brain hemispheres were acquired with the 60× objective. The same exposure settings were used across all conditions in each individual experiment. Images were collected from three old (29–30 months old) wild-type C57BL/6 male mice. Three brain sections were imaged per mouse. Fiji (ImageJ) was used for image analysis. For each image, the presence or absence of T cells was determined by the fluorescence intensity in the CD3 channel. When a T cell was detected, a rectangular area enclosing the T cell and the layers of NSCs lining the ventricle (defined by the SOX2 channel) was manually drawn. A region of the same dimensions was drawn when no T cell was present. The area of the box was kept the same for all samples analysed. These areas were then used to determine the BST2 fluorescence levels by mean intensity across the *Z*-stack. The BST2 intensity was then averaged for each *Z*-stack. The mean intensity BST2 values were normalized for each independent experiment by dividing them by the median intensity of the 'No T cells' values. The *P* value was calculated using the Wilcoxon rank-sum test. Note that BST2 staining was also observed in other cell types, including microglia, in SVZ sections from old mice (Extended Data Fig. 4g).

T cells in human brain specimens: selection, staining and quantification. Human patient samples were obtained from the Stanford University Neuropathology Department. The Stanford autopsy brain bank, which contains brains from Stanford patients who had autopsies with neuropathological examination, was searched over the last 20 years. First, cases that showed no substantial neuropathological abnormalities were selected and classified by age. Cases that did not have appropriate tissue sections of the basal ganglia and cases in which the medical history and other co-morbidities could have an effect on the study were excluded. We excluded patients with neurological or significant neuropathological conditions, immune conditions (including leukaemia, lymphoma, cytokine storm syndrome, severe hepatitis, immunodeficiency and autoimmune disease), ongoing or advanced cancer, recent chemo- or radiotherapy, recent transplants or sepsis. Five young patients (20–44 years old) and six older patients (79–93 years old) of both sexes met the selection criteria and were included for the analysis (Supplementary Table 4).

Formalin-fixed paraffin-embedded brain tissues were sectioned at a thickness of 5 μm and histologic sections were stained with standard haematoxylin–eosin immunohistochemical (IHC) staining. CD3 single-stain IHC was performed using anti-CD3 (Roche Ventana, 2GV6) antibody following the manufacturer's instruction on the Ventana Benchmark Ultra with EDTA pH 8.5 antigen retrieval. For CD8 single-stain IHC, anti-CD8 (Dako Aligent, C8/144B) was used following the manufacturer's instructions on the Leica Biosystem BOND-III Stainer with EDTA pH 9.0 antigen retrieval.

Bright-field images were taken with the 10× objective of an upright Zeiss AxioImager microscope equipped with a ZEISS Axiocam 503 mono camera and Zen Blue software. Image acquisition and analysis were performed blinded. For each sample, the subventricular zone—recognized by the ependymal lining—was imaged. For quantification of T cells, the images were analysed using Fiji (ImageJ). The area lining the ventricle was calculated by drawing a box going 250 μm into the parenchyma. The number of CD3- or CD8-positive T cells within this area was then counted manually for each sample, excluding perivascular T cells, and expressed as the number of T cells per unit area (mm^2). *P* values were calculated using the Wilcoxon rank-sum test.

$CD8^+$ T cell isolation from blood, brain and spleen. For T cell isolation from aged brains, mice were sedated and perfused with 20 ml of PBS with heparin sodium salt (Sigma-Aldrich, 2 mg ml^{-1}) to remove the blood. Brains were immediately collected thereafter. The SVZ was isolated as described above for 'Single-cell RNA-seq using the 10x Genomics Chromium single-cell technology'. Tissue dissociation when isolating pure populations of $CD8^+$ T cells was carried out via a modified protocol from ref. [58] using 2 mg ml^{-1} collagenase type IV (Gibco) for 30 min at 37 °C in HBSS with calcium and magnesium (Gibco), containing 14 μg ml^{-1} of DNase1 (Sigma-Aldrich). The dissociated SVZ was then centrifuged through 22% Percoll (GE Healthcare) in PBS to remove myelin debris. After centrifugation through Percoll solution, cells were washed with FACS buffer (HBSS, 1% BSA, 1% Glucose). Antibody staining was carried out in FACS buffer at the following dilutions: CD45-PE (BioLegend cat. no. 103105, Clone:30-F11 (1:100)), B220-PeCy5 (BioLegend cat. no. 103209, Clone: RA3-6B2 (1:100)), TER119-PeCy5 (BioLegend cat. no. 116209, Clone:TER-119 (1:100)), CD4-APC (BioLegend cat. no. 100411, Clone:GK1.5 (1:100)), CD8-FITC (BioLegend cat. no. 100705, Clone:53-6.7 (1:100)), CD11b-PerCP/Cy5.5 (BioLegend cat. no.101227, Clone:M1/70 (1:100)) and CD3-AF700 (BioLegend cat. no.100216, Clone:17A2 (1:100)). After primary antibody staining, cells were washed with FACS buffer and resuspended in FACS buffer containing 1 μg ml^{-1} DAPI (Thermo Fisher).

To isolate $CD8^+$ T cells from blood, we collected blood samples through a tail vein snip before perfusion. Approximately 50 μl of blood was collected into 250 μl of a 50 U ml^{-1} solution of heparin sodium salt (Sigma-Aldrich), in PBS (Corning). Red blood cells were lysed by adding 2 ml of ACK lysing buffer (Thermo Fisher) for 10 min at room temperature. After lysis of red blood cells, 10 ml of PBS was added to each tube and samples were spun for 10 min at 4 °C. Samples were stained with an identical antibody panel as described above for isolation of $CD8^+$ T cells from the brain.

To isolate $CD8^+$ T cells from the spleen, we removed the spleen and manually dissociated the tissue by chopping repeatedly with a scalpel blade. We then added the manually dissociated spleen to 2 ml of ACK lysing buffer (Thermo Fisher) to lyse the red blood cells. After the lysis of red blood cells, 10 ml of PBS was added to each tube and samples were spun for 10 min at 4 °C. Samples were stained with an identical antibody panel as described above for isolation of $CD8^+$ T cells from the brain.

Smart-seq v4 single-cell RNA-seq of purified brain and blood $CD8^+$ T cells. To characterize T cells from old neurogenic niches, we generated single-cell RNA-seq libraries from $CD8^+$ T cells from the SVZ and blood of four old (25–29 months old) male mice in two independent experiments, performed by two independent investigators (B.W.D. and M.T.B.) (Supplementary Table 7). We also generated libraries from the SVZ of two young (3 months old) mice, although there were very few T cells in the SVZ of young mice (Supplementary Table 7). For library generation, we used the Clontech Smart-seq v4 kit to prepare cDNA. In brief, $CD8^+$ T cells, isolated as described above (defined as $CD45^+CD3^+CD4^-CD8^+B220^-TER119^-CD11b^-$) were clonally sorted into 5 μl of Clontech lysis buffer containing a 1:10,000,000 dilution of ERCC Mix1 (Ambion). cDNA was generated using following the manufacturer's recommendations, as described in the manual (http://www.clontech.com/GQ/Products/cDNA_Synthesis_and_Library_Construction/Next_Gen_Sequencing_Kits/Single_cell_RNA_Seq_Kits_for_mRNA_seq/Single_Cell_RNA_Seq_v4). The only alteration that was made to the protocol was that the reactions were scaled to one-half of the recommended volumes. After cDNA generation, cDNA concentrations were measured using an AATI Fragment analyser. cDNA (50–100 pg) was used as input into the Nextera XT DNA Library Prep Kit (Illumina). The manufacturer's recommendations were followed for the Nextera XT kit, except that all reactions were scaled to one-half of the recommended volumes. The resulting libraries were purified using Agencourt AMPure XP (Beckman Coulter) beads using a 1.8x cleanup. Libraries were multiplexed and sequenced on an Illumina NextSeq-500 (400m), using 75-bp paired-end reads.

Analysis of TCR from Smart-seq single-cell RNA-seq. To test whether T cells from old SVZs were clonally expanded, and whether their TCR repertoire was similar to that of old blood T cells, we analysed the sequence of their TCRs. Paired T cell receptors (TCRα and TCRβ) were reconstructed from $CD8^+$ T-cell Smart-seq v4 full-transcript RNA-seq data using the TraCeR software tool v0.5.1 (https://github.com/teichlab/tracer), described in ref. [59]. In brief, TraCeR maps full-length cDNA reads to all possible combinations of V and J sequences, followed by contig assembly to determine recombined TCR sequences. Productive TCR-α and TCR-β sequences were reconstructed for 199 and 205 of 262 T cells (including 247 old T cells), respectively. TraCeR was run in an Anaconda environment on a Linux-based computing cluster using one node with 16 GB RAM.

TCR and cytokine transcript amplification using nested PCR sequencing. We also used an independent approach, based on nested PCR sequencing, to sequence the TCR and analyse cytokine transcripts from T cells from the SVZ and blood of two old (24 months old) mice and two young (3 months old) mice (Supplementary Table 7). TCR sequencing was performed according to previously established protocols[29]. All primers were designed to have a melting temperature T_m of 70–72 °C ($T_m = 4 \times [GC] + 2[AT]$). All mouse TCR primer sequences are provided in Supplementary Table 13. For TCR primers, base degeneracy was incorporated into the primers when necessary to account for TCR polymorphism and ensure amplification of all known functional Vα, Vβ, Cα and Cβ regions identified in the IMGT database (http://www.imgt.org/). V-region primers were designed to be at least 50 bases from the distal end to ensure inclusion of the entire CDR3 region. All TCR primers for the second reaction contain the common sequence CCAGGGTTTTCCCAGTCACGAC at the 5′ end, which enables amplification with barcoding primers during the third reaction. After all reactions are performed, TCR primers amplify a segment of the TCR of approximately 250 bp. The final product for sequencing is approximately 380 bp. Phenotyping PCR primers were designed to span introns and amplify all major variants of the genes present in the NCBI database (http://www.ncbi.nlm.nih.gov). After the second reaction is performed, phenotyping primers amplify a gene segment of approximately 200 bp, and the final sequencing product is approximately 350 bp.

TCR analysis by nested PCR. TCR sequences from single T cells were obtained by a series of three nested PCR reactions, as described[29]. For all phases of PCR reactions, HotStarTaq DNA polymerase (Qiagen, 203203) was used. The phase 1 PCR reaction was multiplex PCR with multiple Vα and Vβ region primers, Cα and Cβ region primers in a 16-μl reaction. For the phase 1 PCR reaction, the final concentration of each TCR V-region primer is 0.06 μM, each C-region primer is 0.3 μM. A 16-cycle first PCR reaction was performed as per the manufacturer's instructions using the following cycling conditions: 95 °C 15 min; 94 °C 30 s, 62 °C

1 min, 72 °C 1 min × 16 cycles; 72 °C 10 min; 4 °C. Thereafter, a 1-μl aliquot of the phase-1 product was used as a template for 12-μl phase 2 PCR reaction. The following cycling conditions were used for phase-2 PCR: 95 °C 15 min; 94 °C 30 s, 64 °C 1 min, 72 °C 1 min × 25 cycles; 72 °C 5 min; 4 °C. For the phase-2 reaction, multiple internally nested TCRVα, TCRVβ, TCRCα and Cβ primers were used (V primers 0.6 μM, C primers 0.3 μM). The phase-2 primers of TCR V-region contained a common 23-base sequence at the 5′ end to enable further amplification (during the phase-3 reaction) with a common 23-base primer. An aliquot (1 μl) of the phase-2 PCR product was used as a template for the 14-μl phase-3 PCR reaction, which incorporates barcodes and enables sequencing on the Illumina MiSeq platform. For the phase-3 PCR reaction, amplification was performed using a 5′ barcoding primer (0.05 μM) containing the common 23-base sequence and a 3′ barcoding primer (0.05 μM) containing the sequence of a third internally nested Cα and/or Cβ primer, and Illumina Paired-End primers (0.5 μM each). The following cycling conditions were used for phase-2 PCR: 95 °C 15 min; 94 °C 30 s, 66 °C 30 s, 72 °C 1 min × 25 cycles; 72 °C 5 min; 4 °C. The final phase-3 barcoding PCR reactions for TCRα and TCRβ were done separately. For the phase-3 reaction, 0.5 μM of the 3′ Cα barcoding primer and the 3′ Cβ barcoding primer were used. In addition to the common 23-base sequence at the 3′ end (that enables amplification of products from the second reaction) and a common 23-base sequence at the 5′ end (that enables amplification with Illumina Paired-End primers), each 5′ barcoding primer contains a unique 5-base barcode that specifies plate and a unique 5-base barcode that specifies row within the plate. These 5′ barcoding primers were added with a multichannel pipette to each of 12 wells within a row within a plate. In addition to the internally nested TCR C-region sequence and a common 23-base sequence at the 3′ end (that enables amplification with Illumina Paired-End primers), each 3′ barcoding primer contains a unique 5-nucleotide barcode that specifies column. These 3′ barcoding primers were added with a multichannel pipette to each of eight wells within a column within all plates. After the phase-3 PCR reaction, each PCR product should have a unique set of barcodes incorporated that specifies plate, row and column and have Illumina paired-end sequences that enable sequencing on the Illumina MiSeq platform. The PCR products were combined at equal proportion by volume, run on a 1.2% agarose gel, and a band around 350 to 380 bp was excised and gel-purified using a Qiaquick gel extraction kit (Qiagen, 28704). This purified product was then sequenced.

TCR sequencing data was analysed as previously described[29]. In brief, raw sequencing data were processed and demultiplexed using a custom software pipeline to separate reads from every well in every plate as per specified barcodes. All paired ends are assembled by finding a consensus of at least 100 bases in the middle of the read. The resulting paired-end reads are then assigned to wells according to barcode. Primer dimers are filtered out by establishing a minimum length of 100 bases for each amplicon. A consensus sequence is obtained for each TCR gene. Because multiple TCR genes might be present in each well, our software establishes a cutoff of >95% sequence identity within a given well. All sequences exceeding 95% sequence identity are assumed to derive from the same TCR gene and a consensus sequence is determined. The 95% cutoff conservatively ensures that all sequences derived from the same transcript would be properly assigned, even given a PCR rate of 1/9,000 bases, and sequencing error rate up to 0.4%[60] TCR V, D and J segments were assigned by VDJFasta. For phenotyping transcripts, the number of reads containing a 95% match to the customized database of transcription factor and cytokine genes are scored.

Age-associated pathway enrichment analysis. To investigate broad signatures of ageing in each SVZ cell type sequenced, pre-ranked GSEA was carried out using pathways provided in MSigDB Hallmarks v.6.1. The analysis was executed using an R implementation of the Broad Institute's pre-ranked GSEA algorithm (fgsea)[61]. For each cell type, genes were ranked by decreasing MAST derived Z-scores[62] with positive *Z*-scores corresponding to enrichment in old cells.

Fluidigm C1 single-cell RNA-seq of NSC lineage. We also generated Fluidigm C1 single-cell RNA-seq libraries for the NSC lineage. For this experiment, two young (3–4 months old) and two old (20–24 months old) male C57BL/6 mice obtained from the NIA aged colony were euthanized, and brains were immediately collected. As previously described[4], the SVZ from each hemisphere was micro-dissected. The SVZ was dissociated with enzymatic digestion with papain for 10 min at a concentration of 14 U ml^{-1}. The dissociated SVZ was then titrated in a solution containing 0.7 mg ml^{-1} ovomucoid (Sigma-Aldrich), and 0.5 mg ml^{-1} DNaseI (Sigma-Aldrich) in DMEM/F12. The dissociated SVZ was then centrifuged through 22% Percoll in PBS to remove myelin debris. After centrifugation through Percoll solution, cells were washed with FACS buffer (HBSS, 1% BSA, 1% glucose). Antibody staining was carried out in FACS buffer at the following dilutions: Prom1-Biotin (eBioscience cat. no.13-1331-80 (1:300)), CD24-PacBlue (eBioscience cat. no. 48-0242-80 (1:400)), CD31-PE (eBioscience cat. no.12-0311-81 (1:50)), CD45-BV605 (BioLegend cat. no.103139 (1:100)) and O4-APC (Miltenyi cat. no.130-099-211 (1:50)) for 1 hour at 4 °C. Samples were washed with 5 ml of FACS buffer. Secondary staining was performed using Strep-PECy7 (eBioscience cat. no.25-4517-82 (1:500)) in FACS buffer at 4 °C. Samples were washed with 5 ml of FACS buffer, and resuspended in medium containing 1 μg ml^{-1} propidium iodide (BioLegend). Sorting was performed on a BD FACS Aria II sorter, using a 100 μm nozzle at 13.1 psi. Cell gates were defined as follows[4,14,17,20].

NSC-lineage: $PROM1^{+}CD31^{-}CD24^{-}CD45^{-}O4^{-}$ cells were sorted into catching medium: DMEM/F12 with B27 (1:50), B27 supplement (Thermo Fisher, no Vitamin A, 1:50), N2 supplement (Thermo Fisher, 1:100), 15 mM HEPES buffer, 0.6% glucose, penicillin–streptomycin–glutamine (Life Technologies, 1:100), and insulin–transferrin–selenium (Life Technologies, 1:1,000). Cells were then spun down at 300*g* at 4 °C and resuspended in catching medium at a concentration of 300 cells per μl.

A cell solution (300 cells per μl) was mixed at a 7:3 ratio with the Fluidigm C1 Suspension reagent and this solution was loaded onto a small size (5–10 μm) Fluidigm C1 Single-Cell Auto Prep chip for all in vivo single cells studied and medium size (10–17 μm) Fluidigm C1 Single-Cell Auto Prep chip for in vitro cultured neurosphere-derived single cells. Live/dead staining was performed using the Fluidigm Live/Dead Cell Staining Solution as described in the Fluidigm C1 mRNA seq protocol and imaged using a Leica DMI4000B microscope. Reverse transcription was performed directly on the chip using the SMARTer chemistry from Clontech, and PCR was also performed on the chip using the Advantage PCR kit (SMARTer Ultra Low RNA Kit for the Fluidigm C1, Clontech 634832). ERCC spike in mix 1 was included in the lysis buffer at a dilution of 1:100,000 from stock. The resulting cDNA was transferred to a 96-well plate and a subset of representative samples was analysed using a Bioanalyzer system. A quarter of the cDNA for each library was quantified using the Quant-iT PicoGreen dsDNA Assay Kit (Thermo Fisher cat. no. P11496) and verified to be within a range of 0.1–0.5 ng μl^{-1} (or diluted when necessary with the C1 DNA dilution buffer). Sequencing libraries were prepared directly in a 96-well plate using the Nextera XT Library Preparation Kit (Illumina, cat. no. FC-131-1024). Each library was individually barcoded using the Nextera XT 96-Sample Index Kit (Illumina, cat. no. FC-131-1002), and all 96 barcoded libraries from each chip were pooled into single multiplexed libraries. The DNA concentration of multiplexed libraries was measured using the Bioanalyzer. These multiplexed libraries were sequenced using the Illumina MiSeq (Illumina) at a concentration of 2 pM. Details can be found in Supplementary Table 9.

Reads from cells sequenced via the Fluidigm C1 platform were mapped to mm10 using STAR, and gene counts were generated using HTSeq. Cells were excluded from analysis if they were dead on the chip or if fewer than 500 genes were detected in an individual cell.

Principal component analysis with interferon-γ response genes. To test whether single cells exhibit heterogeneous gene expression signatures with respect to interferon-γ response genes, individual PCA plots were generated for specific cell types using genes in the interferon-γ response hallmark gene set from MsigDB (http://software.broadinstitute.org/gsea/msigdb) (Supplementary Table 8). log-transformed and normalized counts for each of the genes in the interferon-γ response hallmark gene set were extracted from the log-transformed normalized gene expression values as calculated by Seurat. A subset of these genes including *Stat1*, *Irf9*, *Ifit1* and *Ifitm3* was verified to be upregulated in cultured NSCs in response to interferon-γ by reverse transcription followed by quantitative PCR, which indicates that NSCs could exhibit a classic transcriptional response to interferon-γ. PCA was then performed with only the genes from this pathway and old cells were visualized using the first two principal components.

Intracellular FACS for STAT1. To stain NSCs and endothelial cells for STAT1, a gene characteristic of the interferon response, the subventricular zone was isolated and dissociated as described above for 'Single-cell RNA-seq using the 10x Genomics Chromium single-cell technology'. Cells in the neural stem cell lineage—including quiescent NSCs, activated NSCs and NPCs—were sorted as a population defined as $PROM1^{+}CD31^{-}CD24^{-}CD45^{-}O4^{-}$, and endothelial cells were defined as $CD31^{+}CD45^{-}O4^{-}$. Each cell type was sorted by FACS into catching medium: DMEM/F12 with B27 (1:50), B27 supplement (Thermo Fisher, no Vitamin A, 1:50), N2 supplement (Thermo Fisher, 1:100), 15 mM HEPES buffer, 0.6% glucose, penicillin–streptomycin–glutamine (Life Technologies, 1:100), and insulin–transferrin–selenium (Life Technologies, 1:1,000). Cells were then centrifuged at 300*g* for 5 min at 4 °C. To perform intracellular FACS on the isolated neural stem cell lineage ($PROM1^{+}CD31^{-}CD24^{-}CD45^{-}O4^{-}$), cells were resuspended in FACS buffer (HBSS, 1% BSA, 1% glucose), and 16% PFA (Thermo Fisher, cat. no. 28906) was added dropwise to the cell suspension to reach a 1.6% final concentration. Cells were fixed in PFA at room temperature for 10 min. Cells were spun down at 500*g* for 5 min and washed twice with FACS buffer. Cells were permeabilized with ice-cold methanol at 4 °C for 10 min. Cells were centrifuged at 500*g* for 5 min and washed twice with FACS buffer. Cells were blocked with DAKO protein block (DAKO) for 30 min at room temperature. Cells were subsequently stained with primary antibodies for STAT1 (Cell Signaling, Clone: D1K9Y (1:100)), and Ki-67 (eBioscience, Clone: SolA15 (1:200)) in FACS buffer overnight at 4 °C. Cells were

washed 3 times with 500 μl of FACS buffer. Cells were stained with the secondary antibodies donkey anti-rat 488 (Thermo Fisher (1:200)), and donkey anti rabbit-PE (Thermo Fisher (1:200)) in FACS buffer for 1 h at 4 °C. Cells were washed 3 times with 0.5 ml FACS buffer. Cells were ultimately resuspended in 100 μl of FACS buffer containing 1 μg ml^{-1} DAPI (Thermo Fisher) and were analysed on a BD LSRII. Cells were analysed in FlowJo.

FACS purification with CD317 (BST2) antibody. The SVZ was isolated and dissociated as described above for 'Single-cell RNA-seq using the 10x Genomics Chromium single-cell technology'. In some cases, mice were given a 1-mg-per-mouse dose of EdU via intraperitoneal injection 4 h before euthanasia. Antibody staining was carried out in FACS buffer at the following dilutions: PROM1-Biotin (eBioscience, cat. no. 13-1331-80 (1:300)), EGF-AlexaFluor 647 (Life Technologies, cat. no. E35351 (1:300)), CD24-PacBlue (eBioscience, cat. no.48-0242-80 (1:400)), CD31-PE (eBioscience, cat. no. 12-0311-81 (1:50)), CD45-BV605 (BioLegend, cat. no. 103139 (1:100)), Strep-PECy7 (eBioscience, cat. no. 25-4517-82 (1:500)), O4-PE (Miltenyi, cat. no. 130-099-211 (1:50)), CD317-FITC (BioLegend, cat. no.127002 Clone:927 (1:50)) for 1 h at 4 °C. Samples were washed with 5 ml of FACS buffer. Secondary staining was performed using Strep-PECy7 (eBioscience, cat. no. 25-4517-82 (1:500)) in FACS buffer at 4 °C. Samples were washed with 5 ml of FACS buffer, and resuspended in medium containing 1 μg ml^{-1} propidium iodide (BioLegend). Fluorescent-minus-one controls were used to set positive gates in each experiment. Cell populations were defined as follows:

qNSCs: $PROM1^+EGFR^-CD31^-CD24^-CD45^-O4^-$

aNSCs/NPCs: $PROM1^+EGFR^+CD31^-CD24^-CD45^-O4^-$

BST2-positive aNSCs/NPCs: $PROM1^+EGFR^+CD31^-CD24^-CD45^-O4^-CD317^+$

BST2-negative aNSCs/NPCs: $PROM1^+EGFR^+CD31^-CD24^-CD45^-O4^-CD317^-$

BST2-positive and BST2-negative aNSCs/NPCs were subjected to subsequent analyses including bulk RNA-seq, EdU/Ki-67 cycle analysis and STAT1 staining.

Bulk RNA-seq of BST2-positive and BST2-negative NSCs. We performed bulk RNA-seq on BST2-positive and BST2-negative aNSCs/NPCs (defined as $PROM1^+EGFR^+CD31^-CD24^-CD45^-O4^-$) from four old (23 months old) C57BL/6 male mice from the NIA aged colony. SVZs were collected and dissociated as described above, and cells were stained as described above in 'FACS with CD317 (BST2) antibody'. Cell identities were defined as follows:

Old BST2-positive aNSCs/NPCs: $PROM1^+EGFR^+CD31^-CD24^-CD45^-O4^-CD317^+$

Old BST2-negative aNSCs/NPCs: $PROM1^+EGFR^+CD31^-CD24^-CD45^-O4^-CD317^-$

Young aNSCs/NPCs: $PROM1^+EGFR^+CD31^-CD24^-CD45^-O4^-$

Because the number of BST2-positive aNSCs/NPCs was low for each old mouse and variable between mice, BST2-positive and BST2-negative aNSCs/NPCs were sorted in groups of five repeatedly until the sample had been exhausted. This process was repeated for each sample derived from independent mice, resulting in matched numbers of BST2-positive and BST2-negative aNSCs/NPCs for each mouse, ranging between 35 and 80 cells per mouse.

To perform the RNA-seq, the Clontech Smart-seq v4 Ultra-Low Input RNA kit (Clontech) was used. Cells were sorted into lysis buffer, as described in the protocol for the kit, and a 1:200,000 dilution of ERCC spike-in mix no. 1 (Ambion) was added. cDNA was prepared as described by the manufacturer. Each cDNA library was analysed on a high-sensitivity chip using an Agilent 2100 Bioanalyzer. To generate sequencing libraries, 0.15 ng of each cDNA library was used as input in the Nextera XT kit, following the manufacturer's recommendations. Cells were indexed using the Nextera XT Index Kit v2 Set A, and were subsequently multiplexed and sequenced on Illumina NextSeq-500 (400m), using 75-bp paired-end reads.

Reads from cells sequenced via the Fluidigm C1 platform were mapped to mm10 using STAR, and gene counts were generated using HTseq.

Pathway enrichment for BST2-positive and BST2-negative RNA-seq. Pathway enrichment was assessed using the GSEA v3.0 algorithm with MSigDB Hallmarks V6.1, similarly to what was done for age-associated enrichment (see above). The only change was that the rank file was generated by sorting genes on the basis of their *Z*-scores calculated from edgeR[63] differential expression analysis results with default settings. Genes with *Z*-scores equivalent to 0 were removed from the ranked list.

EdU analysis of BST2-positive and BST2-negative NSCs. For EdU cell-cycle analysis, BST2-positive and BST2-negative aNSCs/NPCs (defined as $PROM1^+EGFR^+CD31^-CD24^-CD45^-O4^-$) were sorted by FACS into separate wells of a V-bottom 96-well plate containing 100 μl of Neurobasal-A (Thermo Fisher) medium with B27-supplement (Thermo Fisher) (1:50). Cells were washed once with PBS and fixed with 300 μl of ice-cold methanol at 4 °C for 10 min. Click-it chemistry was performed with the Click-iT EdU Alexa Fluor 488 Flow Cytometry Assay Kit (Thermo Fisher) according to the manufacturer's instructions. After the click reaction, cells were washed once with 0.5 ml of FACS buffer, and subsequently stained with 1:100 Ki-67-PE antibody (eBioscience cat. no. 12-5698-82, Clone: SolA15) in FACS buffer for one hour at 4 °C. For measurement of intracellular STAT1, cells were simultaneously stained with STAT1 (Cell Signaling, Clone: D1K9Y (1:100)). After primary antibody staining, cells were washed twice with 0.5 ml of FACS buffer. For measurement of intracellular STAT1, cells were stained with 1:500 donkey anti rabbit-AF568 (Thermo Fisher (1:500)). After secondary staining, samples were washed twice with 0.5 ml of FACS buffer and resuspended in FACS buffer containing 2 μg ml^{-1} Hoechst (Molecular Probes). Samples were analysed on a BD LSRII. Compensation was performed with OneComp eBeads (eBioscience). Final quantification of percentage EdU^+ was only performed on samples that included more than 30 cells.

MOG injection. The injection of MOG was performed according to a previously established protocol used for experimental autoimmune encephalomyelitis[64]. In brief, young male C57BL/6 mice (3 months old) from Jackson Laboratory were injected subcutaneously in the posterior right and left flank with an emulsion containing 200 μg of MOG (Genemed Synthesis, MOG3555-P2-1) and an equal volume of complete Freund's adjuvant (Sigma-Aldrich, F5881) supplemented with 200 μg of *Mycobacterium tuberculosis* H37Ra (Difco Laboratories, 231141). On the day of immunization and 2 days post-immunization, each mouse received 200 ng of Pertussis toxin (List Biological Laboratories, 180) as an adjuvant by intraperitoneal injection. On day 13–15 post-immunization, when mice were exhibiting early symptoms of hindlimb paralysis, the mice were euthanized. In one experiment (MOG experiment 1; Supplementary Table 12), to assess T cell infiltration into the SVZ, the mice were sedated and perfused with 20 ml of PBS with heparin sodium salt (50 U ml^{-1}) (Sigma-Aldrich) to remove the blood, and brains were immediately collected. In the remaining MOG experiments (2, 3, 4 and 5), mice were euthanized without perfusion and the brains were collected. In all experiments, SVZs were micro-dissected as described above. In MOG experiment 1 (Supplementary Table 12), the SVZ was dissected from bilateral hemispheres, the SVZ from one hemisphere was enzymatically processed as described in '$CD8^+$ T cell isolation from blood, brain and spleen' to assess $CD4^+$ and $CD8^+$ T cell infiltration, and the SVZ from the other hemisphere was processed as described in 'FACS purification with CD317 (BST2) antibody', and stained and analysed as described for the remaining MOG experiments described below. T cell FACS analysis was performed as described in '$CD8^+$ T cell isolation from blood, brain and spleen'. For the remaining MOG experiments (MOG experiments 2, 3, 4 and 5, Supplementary Table 12), the samples were processed as described in 'FACS purification with CD317 (BST2) antibody' to assess BST2 status on aNSCs/NPCs. Cell gates for BST2-positive and BST2-negative aNSCs/NPCs were defined as described in 'FACS purification with CD317 (BST2) antibody'. In MOG experiment 4, to perform Ki-67 cell-cycle analysis, BST2-positive and BST2-negative aNSCs/NPCs (defined as $PROM1^+EGFR^+CD31^-CD24^-CD45^-O4^-$) (Extended Data Fig. 7) were sorted by FACS into separate wells of a V-bottom 96-well plate containing 100 μl of Neurobasal-A (Thermo Fisher) medium with B27 supplement (Thermo Fisher) (1:50). Cells were washed once with PBS and fixed with 300 μl of ice-cold methanol at 4 °C for 10 min. Cells were subsequently washed once with 0.5 ml of FACS buffer, and subsequently stained with 1:100 Ki-67-PE antibody (eBioscience cat. no.12-5698-82, Clone: SolA15) in FACS buffer for one hour at 4 °C. Samples were washed twice with 0.5 ml of FACS buffer and resuspended in FACS buffer containing 2 μg ml^{-1} Hoechst (Molecular Probes). Samples were analysed on a BD LSRII. Final quantification of percentage $Ki\text{-}67^+$ was only performed on samples that included more than 30 cells.

Primary cultures of NSCs. To obtain primary cultures of young adult NSCs, the microdissected SVZ from C57BL/6 young male mice (3 months old) from Jackson Laboratory was dissociated with enzymatic digestion with papain for 10 min at a concentration of 14 U ml^{-1}. The dissociated SVZ was then titrated in a solution containing 0.7 mg ml^{-1} ovomucoid (Sigma-Aldrich), and 0.5 mg ml^{-1} DNaseI (Sigma-Aldrich) in DMEM/F12. The dissociated SVZ was then centrifuged through 22% Percoll in PBS to remove myelin debris. After centrifugation through Percoll solution, cells were washed with Neurobasal-A (Thermo Fisher) supplemented with B27-supplement (Thermo Fisher, no Vitamin A, 1:50). Cells were then resuspended in neurospheres cultures and maintained in Neurobasal-A (Thermo Fisher) supplemented with B27-supplement (Thermo Fisher, no Vitamin A, 1:50), penicillin–streptomycin–glutamine (Life Technologies, 1:100), 20 ng ml^{-1} of EGF (Peprotech), 20 ng ml^{-1} of bFGF (Peprotech). To passage cells, they were dissociated for 5 min in Accutase (EMD Millipore) at 37 °C and washed once in PBS (Thermo Fisher), before resuspending the cells in growth medium. To passage neurospheres, neurospheres were spun down at 300*g* for 5 min, and then dissociated by resuspending and incubating for 5 min in 1 ml of Accutase (EMD Millipore). After incubation with Accutase, cells were and washed once in 10 ml PBS (Thermo Fisher). Cells were then resuspended and plated in Neurobasal-A (Thermo Fisher) supplemented with B27-supplement (Thermo Fisher, no Vitamin A, 1:50), penicillin–streptomycin–glutamine (Life Technologies, 1:100), 20 ng ml^{-1} of EGF (Peprotech), 20 ng ml^{-1} of bFGF (Peprotech).

Primary co-cultures of T cells and NSCs. For primary co-cultures of T cells and NSCs, NSCs were isolated as described above. Early passage (P3) neurospheres were dissociated and plated at a density of 10,000 cells per well adherently onto 24-well plates, some containing 12-mm round glass coverslips for immunofluorescence, coated overnight at 37 °C with 20 μg ml^{-1} poly-D-lysine (Sigma-Aldrich) in PBS. Cells were grown for 48 h adherently.

To obtain the high cell number needed for co-cultures, CD8$^+$ T cells were freshly isolated from the spleen of a three-month-old male C57BL/6 mouse obtained from Jackson Laboratory. In brief, the spleen was removed and a small piece of the apex of the spleen was removed and dissociated mechanically by chopping numerous times with a scalpel. The resulting tissue was subjected to red blood cell lysis using 2 ml of ACK lysing buffer (Thermo Fisher) at room temperature for 10 min. Cells were washed with 10 ml of PBS, and were subsequently resuspended in FACS buffer (HBSS, 1% BSA, 0.1% glucose) and filtered through a 35-μm snap-cap filter (Corning). Antibody staining was carried out in FACS buffer at the following dilutions: CD45-PE (BioLegend, cat. no. 103105 Clone:30-F11 (1:100)), B220-PeCy5 (BioLegend, cat. no. 103209 Clone: RA3-6B2 (1:100)), TER119-PeCy5 (BioLegend, cat. no. 116209 Clone:TER-119 (1:100)), CD4-APC (BioLegend, cat. no. 100411 Clone:GK1.5 (1:100)), CD8-FITC (BioLegend, cat. no. 100705 Clone:53-6.7 (1:100)), CD11b-PerCP/Cy5.5 (BioLegend, cat. no.101227 Clone:M1/70 (1:100)), CD3-AF700 (BioLegend, cat. no.100216 Clone:17A2 (1:100)). After primary antibody stain, cells were washed with FACS buffer and resuspended in FACS buffer containing 1 μg ml^{-1} DAPI (Thermo Fisher). CD8$^+$ T cells (defined as CD45$^+$CD3$^+$CD4$^-$CD8$^+$B220$^-$TER119$^-$CD11b$^-$) were sorted into 5 ml of Neurobasal-A medium + 1:50 B27 supplement. T cells were spun at 300*g* for 5 min and resuspended in 1 ml of Neurobasal-A medium.

Before adding T cells to NSC cultures, the medium was changed in each well of NSCs to the medium used to activate T cells. Two approaches were used to achieve T cell activation: (1) the combination of 5 ng ml^{-1} IL2 (carrier free, R&D Systems), and 2 μl of CD3/CD28 Dynabeads (Invitrogen) per well of a 24 well plate; or (2) the combination of 5 ng ml^{-1} IL2 (carrier free, R&D Systems), 20 ng ml^{-1} IL12 (carrier free, R&D Systems), 20 ng ml^{-1} IL18 (carrier free, R&D Systems). All components were added to Neurobasal-A (Thermo Fisher) supplemented with B27-supplement (Thermo Fisher, no Vitamin A, 1:50), penicillin–streptomycin–glutamine (Life Technologies, 1:100), 20 ng ml^{-1} of EGF (Peprotech), 20 ng ml^{-1} of bFGF (Peprotech). When indicated, either 10 μg ml^{-1} anti-interferon-γ antibody (Clone R4-6A2, BioXCell), or 10 μg ml^{-1} Rat IgG1 isotype control (Clone TNP6A7, BioXCell) were included.

For analysis of NSCs upon co-culture with T cells, 2,000 T cells were added to each well of NSCs and the plates were spun at 300*g* for 5 min to sediment T cells on NSC cultures. T cell and NSC co-cultures were left undisturbed for 72 h. After 72 h, cells were incubated with 10 μM EdU for 4 h. For FACS analysis, the cells were detached from the plate by removing the medium and adding 200 μl of Accutase (EMD-Millipore) to each well and incubating at 37 °C for 5 min. Subsequently, cells were split evenly into two tubes. Half of the cells were spun down, washed once with FACS buffer (HBSS, 1% BSA, 1% glucose) and subsequently stained with CD3-AF700 (BioLegend, cat. no.100216 Clone:17A2 (1:100)) and CD317–FITC (BioLegend, cat. no.127002 Clone:927 (1:50)) at 4 °C for one hour. Each tube was washed with 0.5 ml of FACS buffer, spun at 300*g* for 5 min and resuspended in 1 μg ml^{-1} L DAPI (Thermo Fisher) in FACS buffer. The cells were analysed live on an LSRII, excluding DAPI-positive dead cells. Very few T cells were observed in these sorts, even in stimulated conditions—probably because they did not adhere well to the plates and were aspirated away, and because they did not grow well in the NSC medium. Thus, the vast majority of surviving cells were NSCs. The other half of the cells were spun down and fixed with 300 μl of ice-cold 100% methanol at 4 °C for 10 min. They were subsequently washed with 600 μl of FACS buffer. Click-it chemistry was performed with the Click-iT EdU Alexa Fluor 488 Flow Cytometry Assay Kit (Thermo Fisher) according to the manufacturer's instructions. After the click reaction, cells were washed once with 0.5 ml of FACS buffer and subsequently stained with 1:100 Ki67-PE antibody (eBioscience, cat. no.12-5698-82, Clone: SolA15) in FACS buffer for one hour at 4 °C. After antibody staining, samples were washed twice with 0.5 ml of FACS buffer and finally resuspended in FACS buffer containing 2 μg ml^{-1} Hoechst (Molecular Probes). Samples were analysed on a BD LSRII. Compensation was performed with OneComp eBeads (eBioscience). All FACS data analysis was performed in FlowJo.

For immunofluorescence, cells were fixed in 4% PFA in PBS for 15 min at room temperature, followed by permeabilization in 0.2% (v/v) Tween-20 in PBS for 10 min at room temperature. Click-it chemistry was performed with the Click-iT Plus EdU Alexa Fluor 594 Imaging Kit (Thermo Fisher) according to the manufacturer's instructions. After click reaction the cells were washed twice in PBS and were then blocked in 5% normal donkey serum (ImmunoReagents) and 1% BSA (Fisher Biosciences) in PBS for 30 min at room temperature. Primary and secondary antibody stainings were performed in 5% normal donkey serum and 1% BSA in PBS for 1 h at room temperature. Primary antibodies used were the following: BST2 (BioLegend, Clone: 927, (1:200)) and CD3 (Novus Biological, Clone: SP7 (1:200)). The cells were washed three times in blocking buffer after primary antibody staining and twice in blocking buffer, three times in 0.1% Tween-20 in PBS and three times in PBS only after secondary antibody incubation. The coverslips were mounted with ProLong Gold antifade reagent with DAPI (Invitrogen) and imaged with a Nikon Eclipse Ti confocal microscope equipped with a Zyla sCMOS camera (Andor) and NIS-Elements software (AR 4.30.02, 64-bit) using the 60× objective.

Statistical analyses. For most experiments, young and old mice or samples were processed in an alternate manner rather than in two large groups, to minimize the group effect. Although we did not do a bona fide power analysis, we took into account previous experiments to determine the number of animals needed in each experiment. For experiments, all tests were two-sided Wilcoxon rank-sum tests. Results from individual experiments and statistical analysis are included in Supplementary Table 12.

Reporting summary. Further information on research design is available in the Nature Research Reporting Summary linked to this paper.

Data availability

All raw sequencing reads for single-cell RNA-seq data (10x Genomics, Smart-seq v4, and Fluidigm C1) as well as bulk RNA-seq data can be found under BioProject PRJNA450425. The command and configuration files, in addition to a list of all versioned dependencies present in the running environment, are available in the Github repository for this paper (https://github.com/gitbuckley/SingleCellAgingSVZ).

55. Satija, R., Farrell, J. A., Gennert, D., Schier, A. F. & Regev, A. Spatial reconstruction of single-cell gene expression data. *Nat. Biotechnol.* **33**, 495–502 (2015).
56. Doetsch, F., Caillé, I., Lim, D. A., García-Verdugo, J. M. & Alvarez-Buylla, A. Subventricular zone astrocytes are neural stem cells in the adult mammalian brain. *Cell* **97**, 703–716 (1999).
57. Capilla-Gonzalez, V., Cebrian-Silla, A., Guerrero-Cazares, H., Garcia-Verdugo, J. M. & Quiñones-Hinojosa, A. Age-related changes in astrocytic and ependymal cells of the subventricular zone. *Glia* **62**, 790–803 (2014).
58. Jin, Y.-H. & Kim, B. S. Isolation of CNS-infiltrating and resident microglial cells. *Bio Protoc.* **5**, e1385 (2015).
59. Stubbington, M. J. T. et al. T cell fate and clonality inference from single-cell transcriptomes. *Nat. Methods* **13**, 329–332 (2016).
60. Nakamura, K. et al. Sequence-specific error profile of Illumina sequencers. *Nucleic Acids Res.* **39**, e90 (2011).
61. Sergushichev, A. A. An algorithm for fast preranked gene set enrichment analysis using cumulative statistic calculation. Preprint at https://www.biorxiv.org/content/10.1101/060012v1 (2016).
62. Finak, G. et al. MAST: a flexible statistical framework for assessing transcriptional changes and characterizing heterogeneity in single-cell RNA sequencing data. *Genome Biol.* **16**, 278 (2015).
63. Robinson, M. D., McCarthy, D. J. & Smyth, G. K. edgeR: a Bioconductor package for differential expression analysis of digital gene expression data. *Bioinformatics* **26**, 139–140 (2010).
64. Bittner, S., Afzali, A. M., Wiendl, H. & Meuth, S. G. Myelin oligodendrocyte glycoprotein (MOG35-55) induced experimental autoimmune encephalomyelitis (EAE) in C57BL/6 mice. *J. Vis. Exp.* **86**, 51275 (2014).

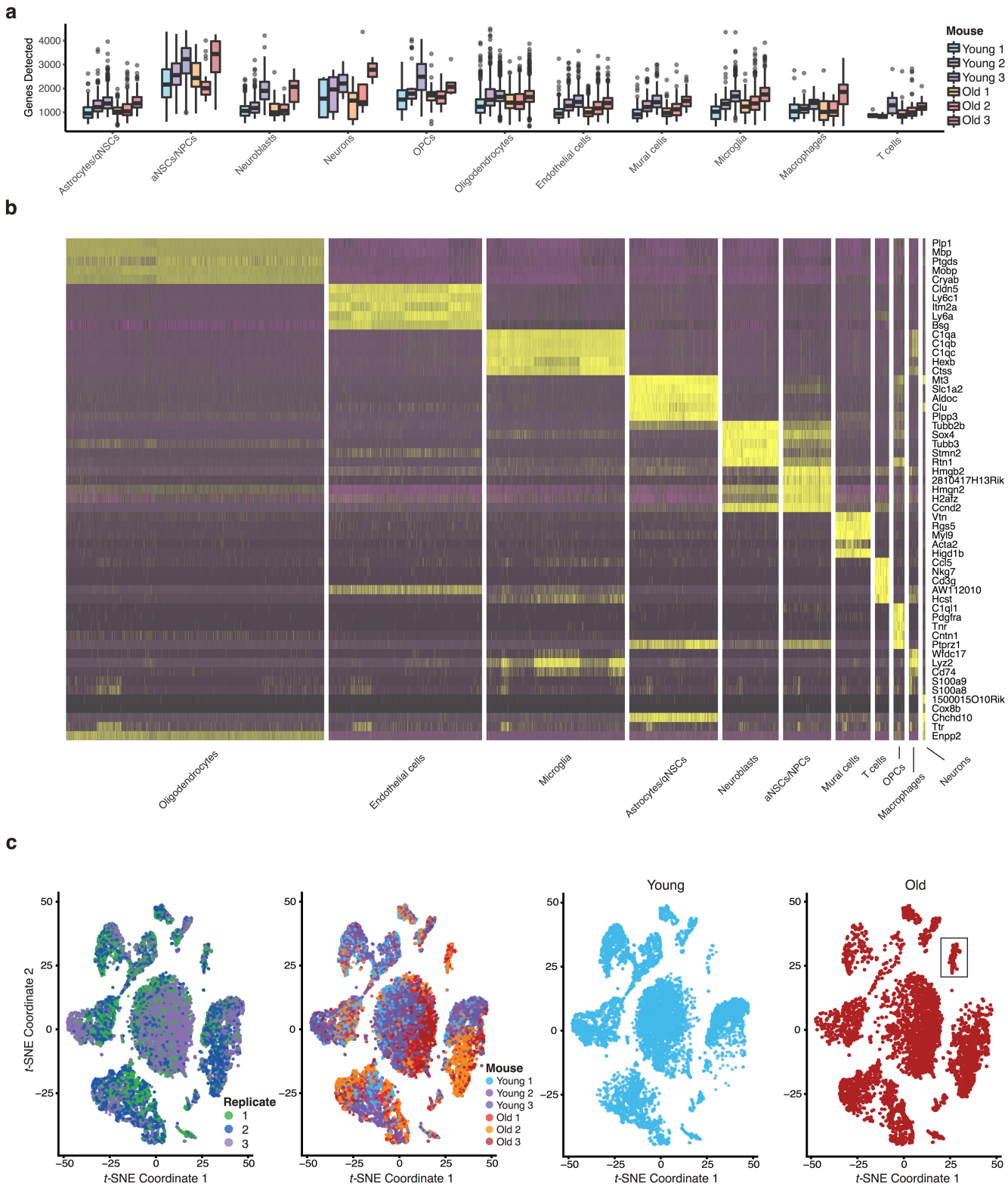

Extended Data Fig. 1 | Quality control for 10x Genomics single-cell RNA-seq data. a, Unique gene counts for 14,685 cells, separated by cell type and individual mouse (complete cell count breakdown available in Supplementary Table 3). Mean ± 25th and 75th percentile are shown by central and outer lines of the boxes; upper and lower whiskers extend to 1.5× of the interquartile range. **b**, Heat map showing the expression of the top five marker genes for each significant cell cluster identified by Seurat. The cell identity assigned to each cluster is indicated on the bottom of each column. **c**, *t*-SNE plots of all 14,685 single-cell transcriptomes analysed by the 10x Genomics platform, coloured by replicates (left), individual mouse (centre), and separated by age (two right-hand plots). Clustering was the same as for Fig. 1a. Eight thousand eight hundred and eighty-four cells from young (young 1, 2,306; young 2, 2,675; young 3, 3,903) and 5,801 cells from old (old 1, 1,435; old 2, 2,541; old 3, 1,825).

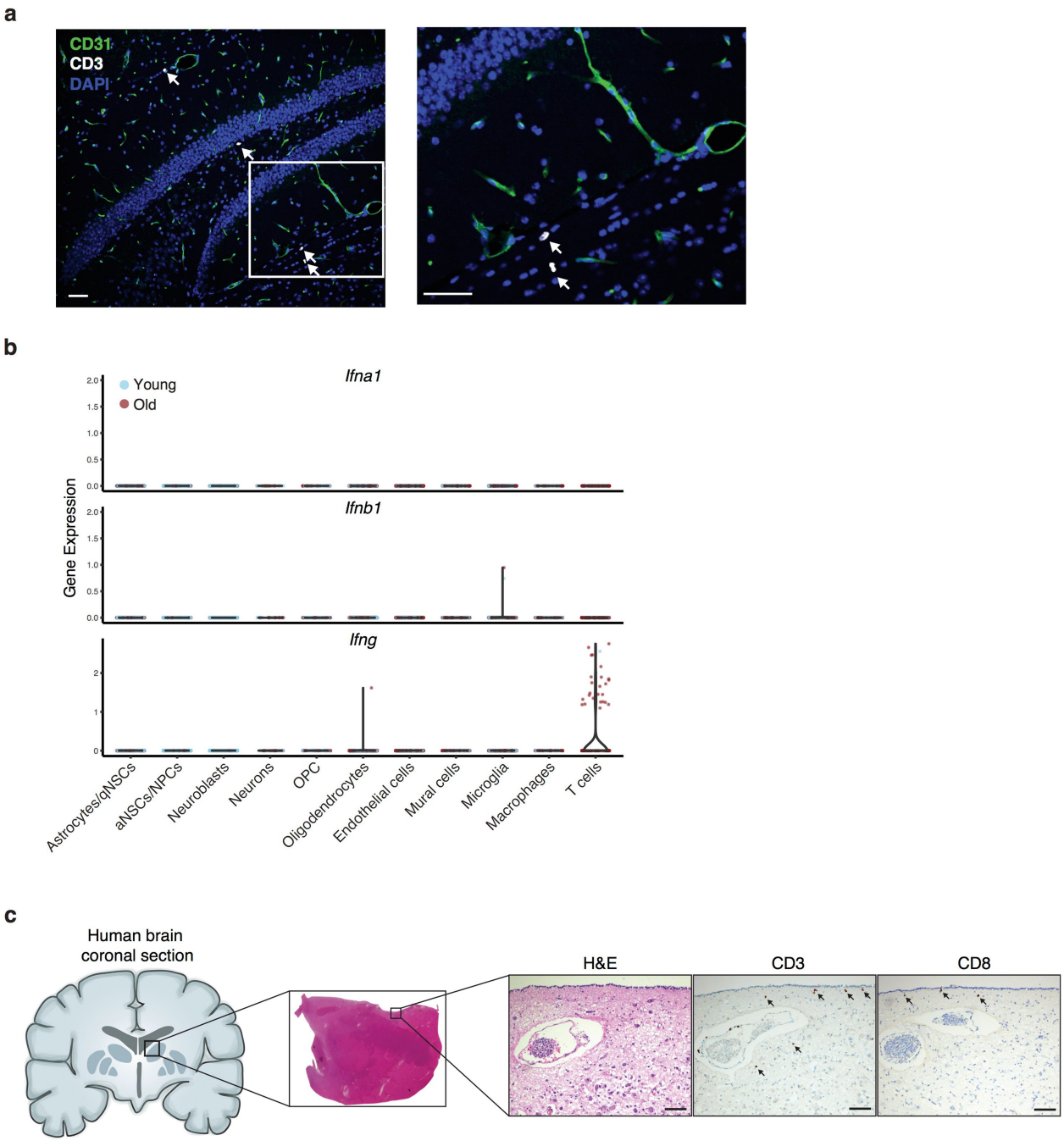

Extended Data Fig. 2 | T cells in old brains are within the brain parenchyma and express *Ifng*. **a**, Immunofluorescence staining of brain sections of the SVZ neurogenic niche from old (24 months old) male mice shows that age-associated T cells do not co-localize with markers of endothelial cells (CD31). Representative of $n = 4$ old mice showing similar results. White, CD3 (T cells); green, CD31 (endothelial cells); blue, DAPI (DNA). The image on the right is an enlarged view of the area in the white square. White arrows point at T cells. Scale bar, 50 μm. **b**, Violin plots showing expression of *Ifna1* (encoding interferon-α), *Ifnb1* (encoding interferon-β) and *Ifng* (encoding interferon-γ) in single cells from different cell types. The data for *Ifng* are also presented in Fig. 1h. Cell types were defined by cell clustering as defined in Fig. 1a. Cells were coloured by age as in Fig. 1b. Expression values are represented as normalized $\log_2$-transformed counts. **c**, Schematic of the experimental design for quantifying T cell infiltration in old human brains. Formalin-fixed paraffin-embedded brain tissue blocks of the basal ganglia with an identifiable ependymal lining (left and middle) from young and elderly humans were sectioned and stained with haematoxylin and eosin or antibodies to CD3 or CD8 for T cell quantification (right). Scale bars, 100 μm.

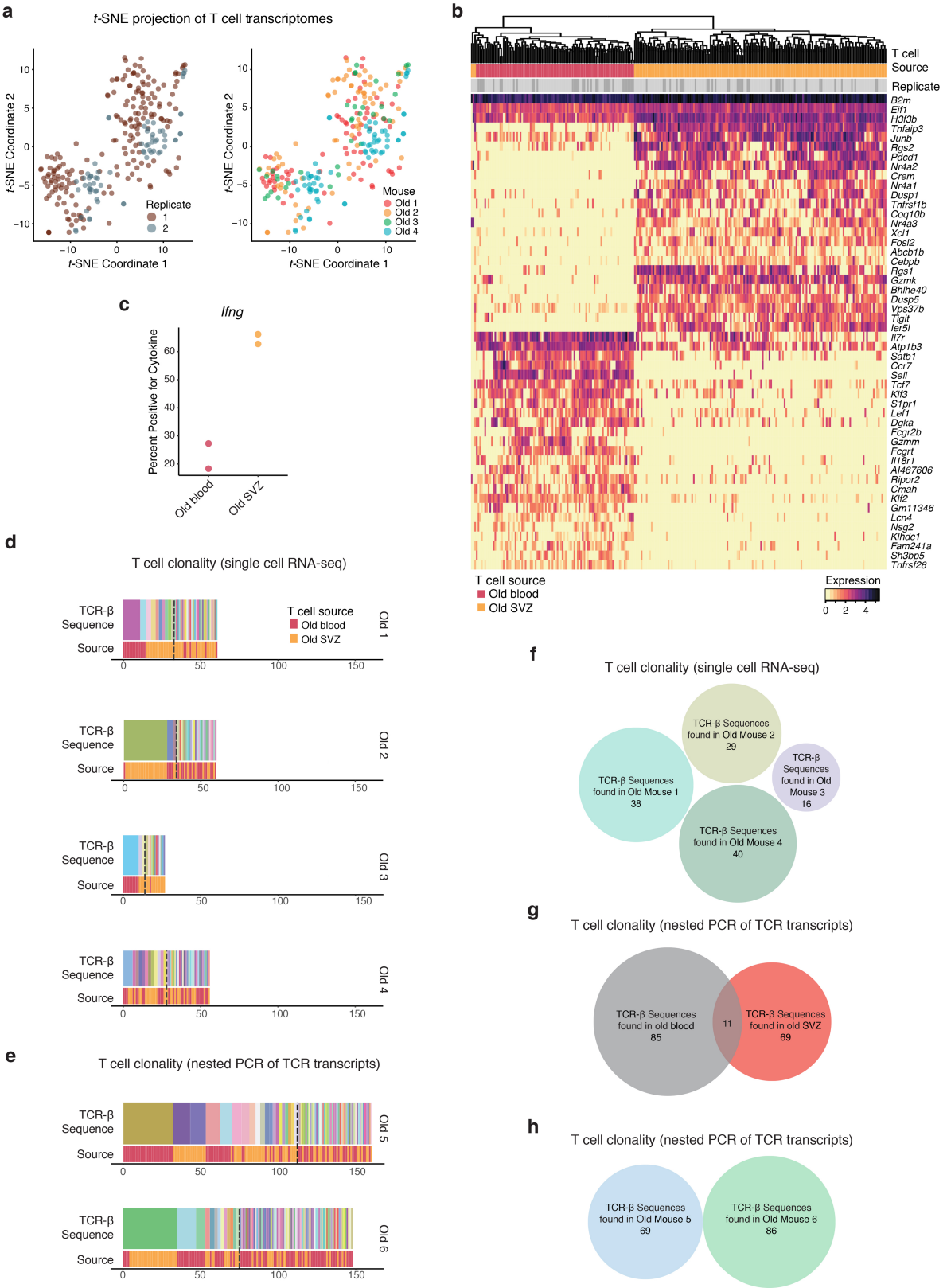

Extended Data Fig. 3 | See next page for caption.

Extended Data Fig. 3 | T cells infiltrating old brains are clonally expanded and differ from T cells in old blood. a, *t*-SNE projections of 247 $CD8^+$ T cell transcriptomes from old blood and old SVZ (as in Fig. 2a), coloured by experimental replicate and individual mouse. **b**, Expression of the top 50 differentially expressed genes upregulated for 247 $CD8^+$ T cells isolated from the blood or SVZ of old mice. Heat map of log-normalized counts, with single cells clustered by the expression of the genes shown in the plot. **c**, Expression of *Ifng* in T cells from blood or SVZs of two old (24 months old) mice, as measured by nested PCR. Data are mean ± s.e.m. of the percentage of T cells that were positive for *Ifng*. Nested PCR does not provide a quantitative metric but rather a binary determination of whether the T cell expresses the transcript for the cytokine or not. **d**, **e**, Clonality of T cells isolated from the blood and perfused brain of old mice, represented with the same *x* axis to enable direct comparison of clone sizes from different mice (the data are the same as Fig. 2c, d). TCR sequences were extracted from single-cell RNA-seq data using TraCer (old mouse 1, 2, 3 and 4) (**d**) or by nested PCR of the TCR transcripts (old mouse 5 and 6) (**e**). For each mouse, TCR-β sequence clones are ordered from left to right in order of decreasing frequency in the top row. The source of the T cell is indicated in the bottom row. **f**, Venn diagram showing the lack of overlap between T cell clones from separate mice, for the four mice for which the TCR repertoire was analysed by single-cell RNA-seq via TraCeR. TCR-β sequences were used, and all unique sequences were only counted once. **g**, **h**, Venn diagram showing the lack of overlap between T cell clones from the old blood and old SVZ (**g**) or from separate mice (**h**), for the two mice for which the TCR repertoire was analysed by nested PCR. TCR-β sequences were used, and all unique sequences were only counted once.

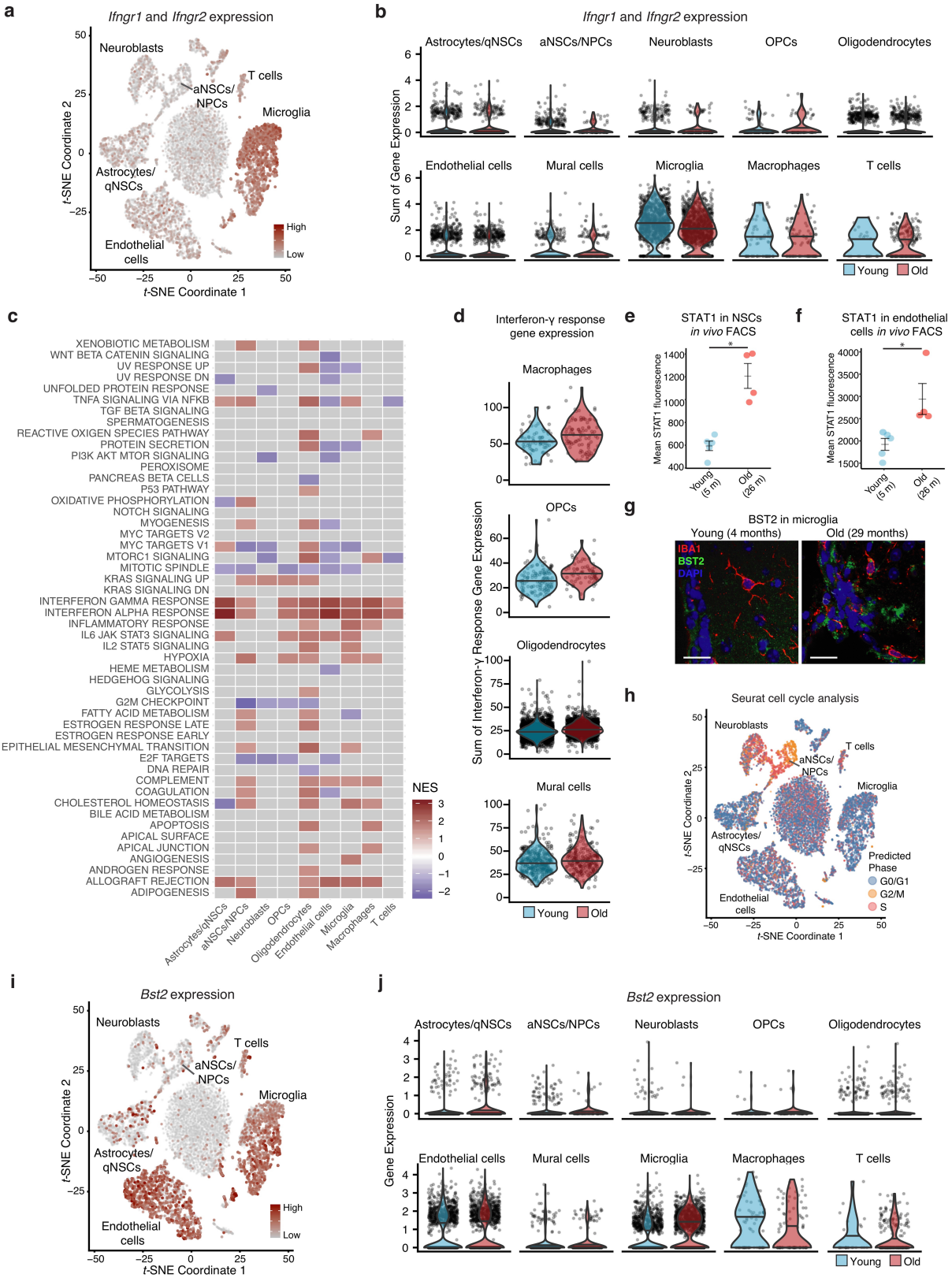

Extended Data Fig. 4 | See next page for caption.

Extended Data Fig. 4 | The neurogenic niche responds to interferon-γ. **a**, *t*-SNE plot showing levels of expression of *Ifngr1* and *Ifngr2* (summed)—which encode the interferon-γ receptor—in 14,685 cells clustered as in Fig. 1a. A darker colour indicates a higher summed expression of *Ifngr1* and *Ifngr2*. Note that there is a lack of correlation between the age-dependent changes in *Ifngr1* and *Ifngr2* levels and changes in the interferon-γ response (Fig. 3a), possibly because of post-transcriptional changes of the interferon-γ receptor. **b**, Violin plots showing expression of *Ifngr1* and *Ifngr2* (summed) by age and cell type. Decrease in microglia is significant at $P < 10^{-15}$ and others are not significant, two-sided Wilcoxon rank-sum test. Horizontal lines in violin plots denote median summed *Ifngr1* and *Ifngr2* expression. See Supplementary Table 3 for exact cell counts. **c**, MSigDB Hallmarks (v.6.1) GSEA results for old compared with young astrocytes/qNSCs, aNSCs/NPCs, neuroblasts, oligodendrocyte progenitor cells, oligodendrocytes, endothelial cells, microglia, macrophages and T cells in the neurogenic niche. The normalized enrichment score is presented for each pathway with FDR < 0.05. Other cell types did not show pathways that met this FDR cutoff. **d**, Combined log-normalized expression values of genes in interferon-γ response hallmark in various cell types of the SVZ. Single cells were grouped by cell type and age (Supplementary Table 3). **e**, FACS analysis of STAT1 levels in the young and old NSCs lineage ($PROM1^+CD45^-CD31^-CD24^-O4^-$), freshly isolated from the brains of five young (5 months old) and four old (26 months old) male mice. Data are mean ± s.e.m. of the mean STAT1 fluorescence of the approximately 500 cells analysed for each mouse. Each dot represents around 500 cells from 1 mouse. $^*P = 0.016$, two-sided Wilcoxon rank-sum test. Data shown are from one experiment (all experiments are plotted in Extended Data Fig. 5d). **f**, FACS analysis of STAT1 levels in endothelial cells freshly isolated from the brains of five young (5 months old) and four old (26 months old) male mice. Data are mean ± s.e.m. of the mean STAT1 fluorescence of the approximately 500 cells analysed for each mouse. Each dot represents around 500 cells from 1 mouse. $^*P = 0.016$, two-sided Wilcoxon rank-sum test. **g**, Immunofluorescence staining of SVZ brain sections from young (4 months old) and old (29 months old) male mice showing BST2 levels in microglia. Green, BST2; red, IBA1 (microglia maker); blue, DAPI. Scale bar, 20 μm. **h**, *t*-SNE plot of 14,685 single-cell transcriptomes with points coloured by putative cell-cycle phase (G0/G1, G2/M or S) as predicted using the CellCycleScoring function in Seurat. **i**, *t*-SNE plot of 14,685 single-cell transcriptomes clustered as in Fig. 1a showing levels of expression of *Bst2* in cells of the SVZ neurogenic niche. Darker colour indicates higher expression of *Bst2*. **j**, Violin plots showing *Bst2* expression by age and cell type. Horizontal lines in violin plots denote median *Bst2* expression. Increase in astrocytes/qNSCs is significant at $P = 6.4 \times 10^{-14}$, increase in oligodendrocytes at $P = 0.025$, increase in microglia at $P < 2.2 \times 10^{-16}$, and others are not significant, two-sided Wilcoxon rank-sum test. See Supplementary Table 3 for exact cell counts.

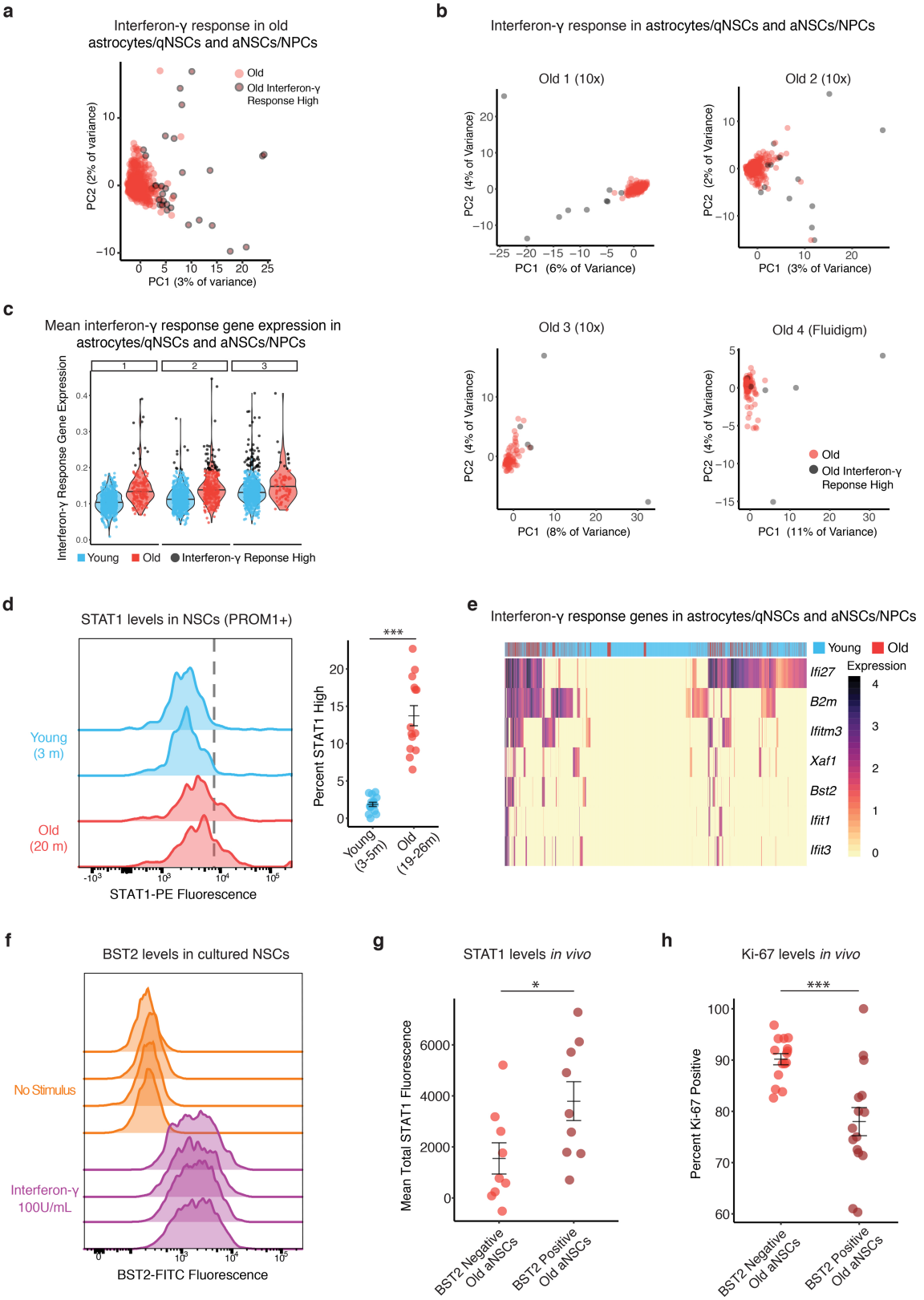

Extended Data Fig. 5 | See next page for caption.

Extended Data Fig. 5 | The old NSC lineage exhibits a heterogeneous response to interferon-γ. a, PCA of 562 old cells in the neural stem cell lineage (astrocytes/qNSCs and aNSCs/NPCs) performed only using genes in the interferon-γ response hallmark from MSigDB (Supplementary Table 8). 'interferon-γ-high' cells (dark red with black ring) are defined as old cells exhibiting an average expression of genes in the interferon-γ response hallmark pathway in the top 5% of old cells. **b**, PCA as in **a**, but with a separate PCA performed for each of three 10x Genomics replicates ($n = 162$, $n = 315$ and $n = 85$ cells) and for the dataset generated with Fluidigm C1 technology ($n = 137$ cells). **c**, Average of normalized expression values of genes in interferon-γ response hallmark for young and old cells in cells of the NSC lineage (astrocytes/qNSCs and aNSCs/NPCs). Cells are grouped by age. Interferon-high cells (in black) are defined as cells that exhibit an average expression of genes in the interferon-γ response hallmark pathway in the top 5% of the cells analysed within each 10x Genomics replicate. Note that replicate three contains approximately twofold more young cells than old cells. Horizontal lines in violin plots denote median interferon-γ response pathway expression. See Supplementary Table 3 for exact cell counts. **d**, FACS analysis of STAT1-positive cells in the young and old NSC lineage ($PROM1^+CD45^-CD31^-CD24^-O4^-$). Left, FACS histograms of STAT1 fluorescence in $PROM1^+$ cells isolated from the SVZ from two representative young (3 months old) and old (20 months old) male mice. Right, quantification of the percentage of STAT1-high cells in 15 young (3–5 months old) and 14 old (19–26 months old) mice. Data are mean ± s.e.m. of the percentage of cells that are STAT1-high of the approximately 500 cells analysed for each mouse. Each dot represents approximately 500 cells from 1 mouse. The combined results from five independent experiments are shown (for independent experiments, see Supplementary Table 12). $^{***}P = 5.08 \times 10^{-6}$, two-sided Wilcoxon rank-sum test. **e**, The gene encoding the surface marker BST2 is expressed in the old NSC lineage and is correlated with genes that belong to interferon-γ signalling. Data are shown as a heat map with log-normalized expression of *Bst2* and other select genes in the interferon-γ response hallmark pathway. Cells are clustered on the basis of expression of this gene set. The ages of the mice from which the cells are isolated is indicated in a bar above the heat map. **f**, Live FACS analysis for BST2 in cultured NSCs after interferon-γ treatment for 48 h. **g**, Abundance of total STAT1 protein in BST2-positive compared with BST2-negative aNSCs/NPCs isolated from nine old (25 months old) mice, as measured by intracellular FACS. Data are mean ± s.e.m. of total STAT1 fluorescence. Each dot represents cells from one mouse. The combined results from two independent experiments are shown (for independent experiments, see Supplementary Table 12). $^{*}P = 0.04$, two-sided Wilcoxon rank-sum test. **h**, FACS quantification for Ki-67, a marker of cycling cells, in BST2-positive and BST2-negative aNSCs/NPCs from 15 old (23–25 months old) mice. Data are mean ± s.e.m. of percentage of cells that are Ki-67 positive of the approximately 100 cells analysed for each mouse. Each dot represents around 100 cells from 1 mouse. The combined results from three independent experiments are shown (for independent experiments, see Supplementary Table 12). $^{***}P = 7.80 \times 10^{-4}$, two-sided Wilcoxon rank-sum test.

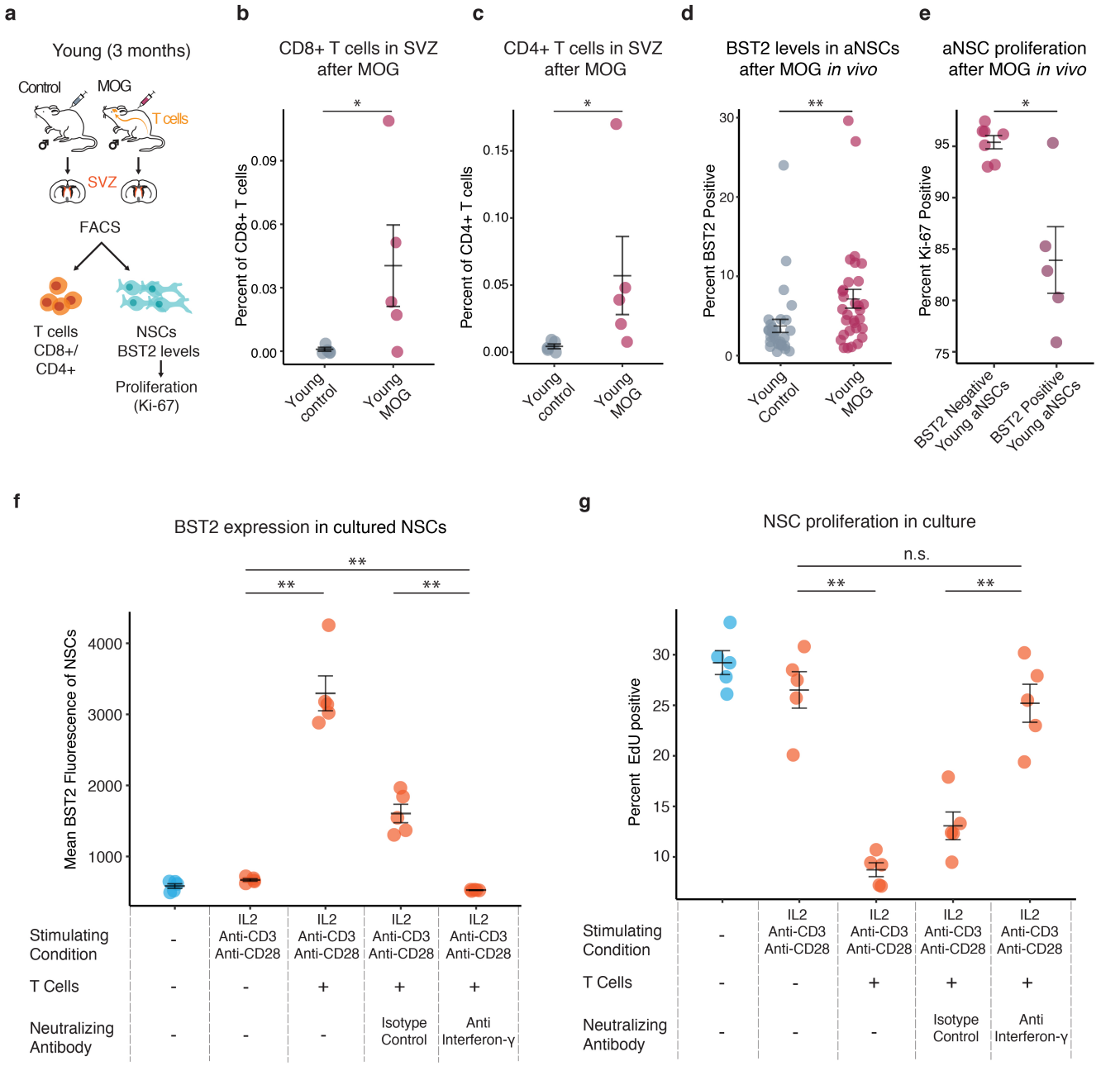

Extended Data Fig. 6 | T cells can influence NSCs in vivo and in co-cultures. a, Schematic showing the induction of T cell infiltration of the brains of young mice by immunization with recombinant MOG. NSCs were purified 13–15 days after MOG immunization, and BST2 levels and proliferative (cycling) status (as determined by intracellular Ki-67 levels) of NSCs were measured by FACS. **b**, **c**, FACS analysis of $CD8^+$ (**b**) and $CD4^+$ (**c**) T cells freshly isolated from the brains of five control or five MOG-injected young mice (3 months old). Data are mean ± s.e.m of the percentage of live cells that are defined as $CD8^+$ or $CD4^+$ T cells, defined as $CD3^+CD45^+TCR\gamma/\delta^-B220^-TER119^-CD11b^-$. $^*P = 0.016$ (**b**), $^*P = 0.045$ (**c**), two-sided Wilcoxon rank-sum test. Each dot represents one mouse. **d**, Percentage of aNSCs/NPCs that are BST2-positive sorted from 30 young (3 months old) male mice injected with adjuvant (control) and 31 young (3 months old) male mice injected with adjuvant with MOG (see 'MOG injection' in Methods), combined over five experiments (for individual experiments, see Supplementary Table 12). Data are mean ± s.e.m. of the percentage of cells that are BST2-positive of the approximately 500 cells analysed from each mouse. Each dot represents cells from one mouse. $^{**}P = 0.002$, two-sided Wilcoxon rank-sum test. **e**, FACS analysis for Ki-67 in freshly isolated BST2-positive and BST2-negative aNSCs/NPCs sorted from 7 young mice (3 months old) that were injected with MOG. Data are mean ± s.e.m. of the percentage of cells that are Ki-67-positive of the approximately 100 cells analysed from each mouse. Samples were excluded if there were fewer than 30 intact cells analysed in a given sample (resulting in 7 samples for BST2-negative and 5 samples for BST2-positive aNSCs/NPCs). Each dot represents cells from one mouse. $^*P = 0.018$, two-sided Wilcoxon rank-sum test. **f**, **g**, BST2 levels and EdU incorporation in cultured NSCs after co-culture with spleen $CD8^+$ T cells incubated with a combination of IL2, along with beads coated with anti-CD3 and anti-CD28 antibodies, which are known to activate $CD8^+$ T cells. **f**, BST2 levels in NSCs, measured by live FACS analysis, plotted as mean BST2 fluorescence. **g**, Percentage of NSCs incorporating EdU, a nucleotide analogue, during a 4-h pulse of EdU. The effects of activated T cells on NSCs are reversed by the addition of a neutralizing antibody to interferon-γ. Data are mean ± s.e.m. of the percentage of cells that are BST2-positive or EdU-positive of the approximately 1,000 cells analysed from each NSC culture. Each dot represents an independent culture of NSCs, derived from a separate mouse ($n = 5$). Data are from one independent experiment (see Supplementary Table 12). $^{**}P = 0.008$, n.s. = not significant, two-sided Wilcoxon rank-sum test.

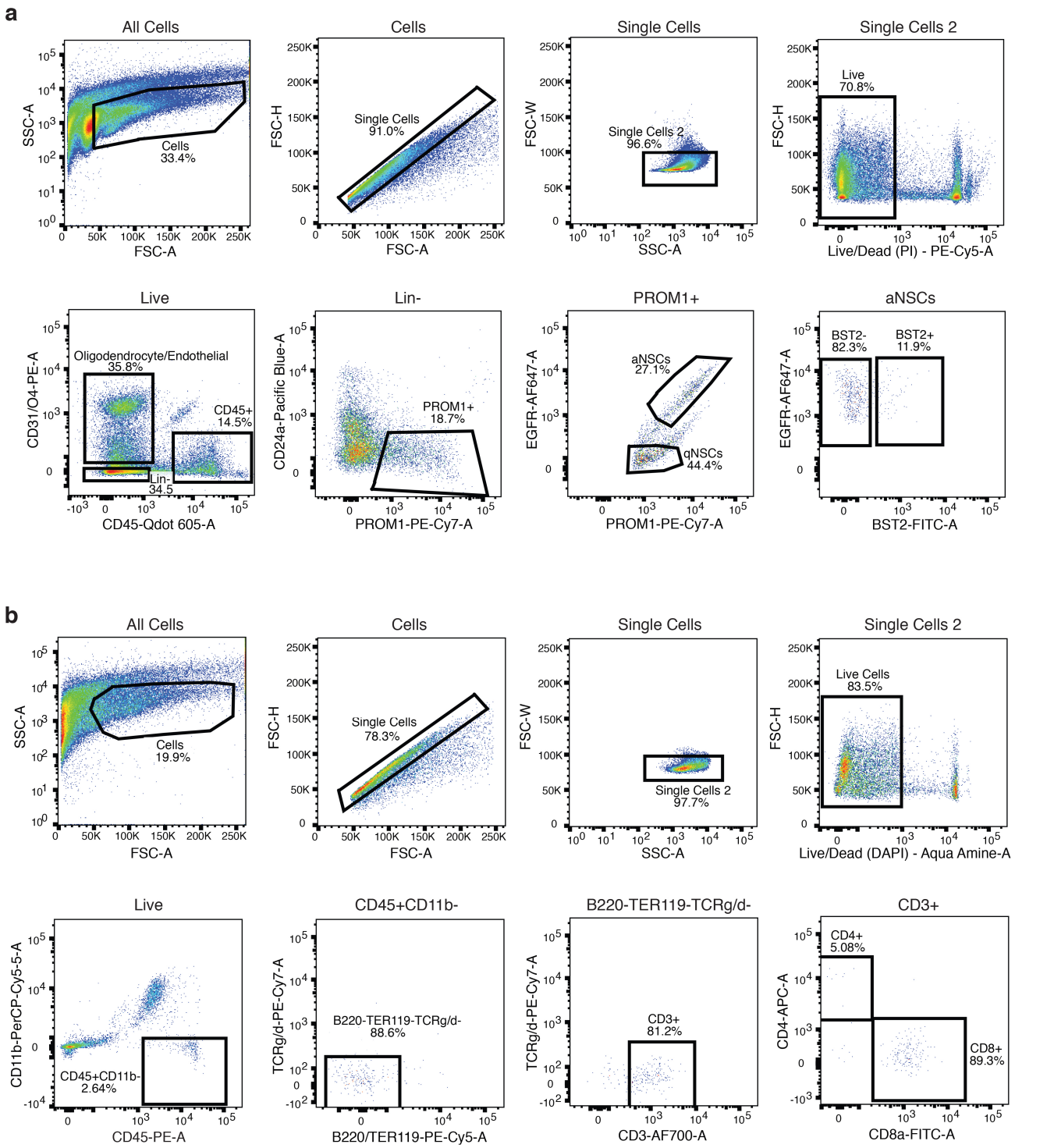

Extended Data Fig. 7 | FACS gating strategies. a, FACS scheme for the isolation of PROM1$^+$EGFR$^+$CD45$^-$CD31$^-$O4$^-$CD24a$^-$ aNSCs/NPCs from the adult SVZ. The gate shown on each plot is indicated above the plot. Marker and fluorophore are shown on each axis. **b**, FACS scheme for the isolation of CD8$^+$CD4$^-$CD3$^+$CD45$^+$TCRγ/δ^-B220$^-$TER119$^-$CD11b$^-$ T cells from adult SVZ, spleen and blood. The gate shown on each plot is indicated above the plot. The marker and the fluorophore are shown on each axis.

nature research

Corresponding author(s): Anne Brunet

Last updated by author(s): Mar 29, 2019

Reporting Summary

Nature Research wishes to improve the reproducibility of the work that we publish. This form provides structure for consistency and transparency in reporting. For further information on Nature Research policies, see Authors & Referees and the Editorial Policy Checklist.

Statistics

For all statistical analyses, confirm that the following items are present in the figure legend, table legend, main text, or Methods section.

n/a	Confirmed
☐	☒ The exact sample size (*n*) for each experimental group/condition, given as a discrete number and unit of measurement
☐	☒ A statement on whether measurements were taken from distinct samples or whether the same sample was measured repeatedly
☐	☒ The statistical test(s) used AND whether they are one- or two-sided *Only common tests should be described solely by name; describe more complex techniques in the Methods section.*
☐	☒ A description of all covariates tested
☐	☒ A description of any assumptions or corrections, such as tests of normality and adjustment for multiple comparisons
☐	☒ A full description of the statistical parameters including central tendency (e.g. means) or other basic estimates (e.g. regression coefficient) AND variation (e.g. standard deviation) or associated estimates of uncertainty (e.g. confidence intervals)
☐	☒ For null hypothesis testing, the test statistic (e.g. *F*, *t*, *r*) with confidence intervals, effect sizes, degrees of freedom and *P* value noted *Give P values as exact values whenever suitable.*
☒	☐ For Bayesian analysis, information on the choice of priors and Markov chain Monte Carlo settings
☒	☐ For hierarchical and complex designs, identification of the appropriate level for tests and full reporting of outcomes
☒	☐ Estimates of effect sizes (e.g. Cohen's *d*, Pearson's *r*), indicating how they were calculated

Our web collection on statistics for biologists contains articles on many of the points above.

Software and code

Policy information about availability of computer code

Data collection	NIS-Elements software (version AR 4.30.02), BD FACSDiva software (version 8.0.1), Zen blue edition (version 2.3)
Data analysis	Data analysis was performed using R version 3.4.3. Packages used include: Seurat (version 2.3.4) , EdgeR (version 3.16.5), fgsea (version 1.4.1), MAST (version 1.4.1), cellrangerRKit (version 1.1.0), ggplot2 (version 3.1.0), venneuler (version 1.1-0), TraCeR (version 0.5.1), , ggpubr (version 0.1.7), STAR (version 2.5.3a), gplots (version 3.0.1), clusterProfiler (version 3.6.0), biomaRt (version 2.34.2). FlowJo (version 10.2), ImageJ (version 2.0.0), Enricher (http://amp.pharm.mssm.edu/Enrichr/).

For manuscripts utilizing custom algorithms or software that are central to the research but not yet described in published literature, software must be made available to editors/reviewers. We strongly encourage code deposition in a community repository (e.g. GitHub). See the Nature Research guidelines for submitting code & software for further information.

Data

Policy information about availability of data

All manuscripts must include a data availability statement. This statement should provide the following information, where applicable:

- Accession codes, unique identifiers, or web links for publicly available datasets
- A list of figures that have associated raw data
- A description of any restrictions on data availability

Sequencing data that support the findings of this study have been deposited in NCBI BioProject database under the accession code PRJNA450425. Figures 1-4 of this study are all associated with raw data which can be found under this accession number. For Figure 1, raw output bam files for 10x single cell RNA-sequencing are provided. For Figure 2, raw sequences for single cell RNA-sequencing of brain and blood associated CD8+ T cells are provided as fastq files. For Figure 4, raw sequencing data for the sequencing of young and old single neural stem cells on the Fluidigm C1 platform are provided as fastq files. For Figure 4, raw sequencing data for the sequencing of BST2+ and BST- neural stem cells are provided as fastq files.

Field-specific reporting

Please select the one below that is the best fit for your research. If you are not sure, read the appropriate sections before making your selection.

☒ Life sciences ☐ Behavioural & social sciences ☐ Ecological, evolutionary & environmental sciences

For a reference copy of the document with all sections, see nature.com/documents/nr-reporting-summary-flat.pdf

Life sciences study design

All studies must disclose on these points even when the disclosure is negative.

Sample size	The sample size was decided based on previous experiments (but we did not do a power analysis and have clearly indicated this in Materials and Methods (Statistics section). In cases where samples from independent experiments were combined, we have clearly indicated this, and the non-combined data are provided in a Supplementary Table 12.
Data exclusions	All data is included in the current study.
Replication	All attempts at replication were successful. Independent replication was done for Fig. 1a,b,c,d,f,g,h,i,j,k,m, Fig. 2a,b,c,d,,f,g, Fig. 3a,b,c,d,e, Fig. 4a,b,d,f,h part of k,l,m. Extended Data Fig. 1a,b,c, Extended Data Fig. 2b, Extended Data Fig. 3a,c,e, Extended Data Fig. 4a,b,c,g,h,i, Extended Data Fig. 5a,b,d,f,g, Part of Extended Data Fig. 6c,d (the IFN blockade was not performed in replicate). All of the independent experiments are presented in a supplementary table (Supplementary Table 12) and this is indicated in figure legends. We also note that for those experiments that were not directly independently replicated, we included an orthogonal validation (Fig. 2e, Fig. 4c,i, Extended Data Fig. 3b,d,f,g, Extended Data Fig. 4d,e,f, Extended Data Fig 5 d, Extended Data Fig. 6a,b).
Randomization	When possible, mice from multiple mice orders from the NIA were randomized and used in experimental groups.
Blinding	Blinding was done for Fig. 1m. Blinding was not done for the rest of the figures. However, note that all the quantification (except Fig. 1f and g and Fig. 4f) were done via FACS or automated image quantification. We have indicated that no blinding was done for these figures in Materials and Methods.

Reporting for specific materials, systems and methods

We require information from authors about some types of materials, experimental systems and methods used in many studies. Here, indicate whether each material, system or method listed is relevant to your study. If you are not sure if a list item applies to your research, read the appropriate section before selecting a response.

Materials & experimental systems

n/a	Involved in the study
☐	☒ Antibodies
☒	☐ Eukaryotic cell lines
☒	☐ Palaeontology
☐	☒ Animals and other organisms
☐	☒ Human research participants
☒	☐ Clinical data

Methods

n/a	Involved in the study
☒	☐ ChIP-seq
☐	☒ Flow cytometry
☒	☐ MRI-based neuroimaging

Antibodies

Antibodies used	Antibodies used for immunofluorescence: BST2 (BioLegend, Clone: 927, Cat.# 127016, Lot: B256699, [1:200]), CD3 (Novus Biological, Clone: SP7, Cat.# NB600-1441, Lot: L139 and J275, [1:200], CD31 (R&D Systems, Cat.# AF3628, Lot: YZU0117021, [1:500]), IBA1 (Novus Biological, Cat.# NB100-1028, Lot: S7C7G2P24-E250517, [1:500], KI67 (eBioscience, Clone: SolA15, Cat.# 50245564, Lot: 4328926, [1:500]), SOX2 (R&D Systems, Cat.# AF2018, Lot: KOY0317071, [1:200]), STAT1 (Cell Signaling, Cat.# 7649, Clone: D1K9Y, Lot: 4 [1:500]). Antibodies used for IHC in human brain samples: anti-CD8 (Dako Aligent, Clone: C8/144B, Cat.# GA62361-2, Lot: 20042547), anti-CD3 (Roche Ventana, Clone: 2GV6, Cat.# 790-4341, Lots: E13640, E19428 and E27059). Antibodies used to block IFN gamma: InVivoMAb rat anti-IFN gamma antibody (BioXCell, Clone: R4-6A2, Cat. # BE0054, Lot: 601516A2, [10µg/mL]), InVivoMAb rat anti-IgG1 isotype control (BioXCell, Clone: TNP6A7, Cat. # BE0290, Lot: 680918F1, [10µg/mL]). Secondary antibodies: donkey anti rabbit-AF568 (ThermoFisher, Cat.# A10042, Lot:1964370, [1:500]), donkey anti rat-AF488 (ThermoFisher, Cat.# A21208, Lot: 1900239, [1:500]), donkey anti goat-AF647 (ThermoFisher, Cat.# A21447, Lot:1841382, [1:500]).

Antibodies used for FACS: CD45-PE (Biolegend Cat.# 103105 Clone:30-F11 Lot: B237529 [1:100]), B220-PeCy5 (Biolegend Cat.# 103209 Clone:RA3-6B2 Lot:B213875 [1:100]), TER119-PeCy5 (Biolegend Cat.# 116209 Clone:TER-119-PeCy5 Lot:B247523 [1:100]), CD4-APC (Biolegend Cat.# 100411 Clone:GK1.5 Lot:B237268 [1:100]), CD8-FITC (Biolegend Cat.# 100705 Clone:53-6.7 Lot:B240641 [1:100]), CD11b-PerCP/Cy5.5 (Biolegend Cat.#101227 Clone:M1/70 Lot:B260458 [1:100]), CD3-AF700 (Biolegend Cat.#100216 Clone:17A2 Lot:B248690 [1:100]), Prom1-Biotin (eBioscience Cat.#13-1331-80 Clone: 13A4 Lot:2025235 [1:300]), EGF-AlexaFluor 647 (Life Technologies Cat. #E35351 Lot: 1917932 [1:300]), CD24-PacBlue (eBioscience Cat.#48-0242-80 Clone:M1/69 Lot:E08500-1633 [1:400]), CD31-PE (eBioscience Cat.#12-0311-81 Clone:390 Lot:4338515 [1:50]), CD45-BV605 (Biolegend Cat.#103139 Clone: 30-F11 Lot:B250086 [1:100]), Strep-PECy7 (eBioscience Cat.#25-4517-82 Lot:E07615-1631 [1:500]), O4-PE (Miltenyi Cat.#130-099-211 Clone:O4 Lot:5180327405 [1:50]), CD317-FITC (Biolegend Cat.#127002 Clone:927 Lot:B268040 [1:50]), TCRγδ-PeCy7 (Biolegend, Cat.#118123 Clone:GL3 Lot:B254396 [1:100]), KI67-PE (eBioscience, Cat.#12-5698-80 Clone:SolA15 Lot:1923633 [1:100].

Validation

The STAT1 and BST2 antibodies were validated in cultured NSCs by performing knockouts with CRISPR/Cas9 followed by FACS. We also used cultured NSCs with stimulation with IFN to verify that the STAT1 and BST2 antibodies were indeed recognizing cells that were treated with IFN.

We verified that the anti-CD3 antibody did indeed stain the cell membrane exclusively, as expected. The antibody was also validated via knockdown by the manufacturer.

Antibody staining of CD31 resulted in marking of structures bearing the morphology of blood vessels, as expected and as shown by the manufacturer. More than 60 citations used this antibody.

Antibody staining of IBA1 resulted in marking of structures bearing the morphology of microglia, as expected and as shown by the manufacturer and 30 publications using this antibody.

KI67 antibody only stained the nuclei of dividing activated NSCs and not quiescent NSCs in vitro, functionally validating the antibody. It was also used in 84 published papers.

SOX2 staining was nuclear as expected. Used in 72 citations.

The anti-CD8 (Dako Aligent, C8/144B) and anti-CD3 (Roche Ventana, 2GV6) antibodies were validated in house following the College of American Pathologist recommendations. Briefly the validation is done in house using 20 negative controls and 20 positive controls with low, moderate and high expression levels of the antigen from appropriately formalin fixed and paraffin embedded tissue. Validated protocols and antibodies have at least a 90% concordance with the expected results. All new lots are tested before use. All controls showed appropriate reactivity.

The anti-IFNg and anti-IgG antibodies were validated by the manufacturer.

FACS sorted population isolated in this study were analyzed by RNA-sequencing, which enabled us to validate antibodies by ensuring that populations sorted as positive for certain markers did indeed exhibit expression of those associated markers, which in the case of this study was observed for all populations and antibodies used in this study.

All antibodies used for T cell FACS (CD45-PE, B220-PeCy5, TER-119-PeCy5, CD4-APC, CD8-FITC, CD11b-PerCP/Cy5.5, CD3-AF700) were validated by the manufacturer and widely cited in the literature.

Animals and other organisms

Policy information about studies involving animals; ARRIVE guidelines recommended for reporting animal research

Laboratory animals

All mice used in this study were male C57BL/6 obtained from the NIA Aged Rodent colony with ages ranging from 3-6 months for young adult animals and 24-30 months for old animals (precise ages are stated for each experiment in Supplementary Data Table 12). All cultured NSCs come from young mice (3 months) from Jackson. Mice were habituated for >1 week at Stanford before use. At Stanford, all mice were housed in the Comparative Medicine Pavilion or the Research Animal Facility II and their care was monitored by the Veterinary Service Center at Stanford University under IUCAC protocols #8661 and #28396.

Wild animals

No wild animals were used in this study.

Field-collected samples

No field-collected samples were used in this study.

Ethics oversight

At Stanford, all mice were housed in the Comparative Medicine Pavilion or the Research Animal Facility II and their care was monitored by the Veterinary Service Center at Stanford University under IUCAC protocols #8661 and #28396.

Note that full information on the approval of the study protocol must also be provided in the manuscript.

Human research participants

Policy information about studies involving human research participants

Population characteristics

Five young patients between 20 and 44 years and 6 older patients between 79 and 93 years of both sexes were included for the analysis (Supplementary Table 4).

Recruitment

Human patient samples were obtained from the Stanford University Neuropathology Department. The Stanford autopsy brain

Recruitment	bank, which contains brains from Stanford patients that have had autopsies with neuropathological examination, was searched over the last 20 years. First, cases that showed no significant neuropathological abnormalities were selected and classified by age. Cases that did not have appropriate tissue sections of the basal ganglia and cases where the medical history and other comorbidities could have impact on the study were excluded including patients with neurological or significant neuropathological conditions, immune conditions (including leukemia, lymphoma, cytokine storm syndrome, severe hepatitis, immunodeficiency and autoimmune disease), ongoing or advanced cancer, recent chemo or radio therapy, recent transplants or sepsis.
Ethics oversight	The Stanford University IRB determined that an IRB protocol was not required since the research involved cadavers, autopsy material or biospecimens from deceased individuals rather than living individuals.

Note that full information on the approval of the study protocol must also be provided in the manuscript.

Flow Cytometry

Plots

Confirm that:

☒ The axis labels state the marker and fluorochrome used (e.g. CD4-FITC).

☒ The axis scales are clearly visible. Include numbers along axes only for bottom left plot of group (a 'group' is an analysis of identical markers).

☒ All plots are contour plots with outliers or pseudocolor plots.

☒ A numerical value for number of cells or percentage (with statistics) is provided.

Methodology

Sample preparation	For sorting of primary neural stem cells from the neural stem cell niche: For single cell RNA-sequencing of all live cells in the SVZ neurogenic niche, two young (3-4 months), and two old (24-29 months) male C57Bl6 mouse from the NIA aged colony were used in two independent experiments. Mice were sedated and perfused with 20 ml of PBS, and brains were immediately harvested. As described in 34, the SVZ from each hemisphere was microdissected and dissociated with enzymatic digestion with papain for 10 min at a concentration of 14U/mL. The dissociated SVZ was then titrated in a solution containing 0.7mg/mL ovomucoid, and 0.5 mg/mL DNAseI in DMEM/F12. The dissociated cells from the SVZ were then centrifuged through 22% Percoll in PBS to remove myelin debris. Following centrifugation through Percoll solution, cells were washed with FACS buffer (HBSS, 1% BSA, 1% Glucose). Live/dead staining was performed using 1µg/mL propidium iodide (Biolegend). FACS sorting was performed on a BD FACS Aria II sorter, using a 100µm nozzle at 13.1 PSI. Cells were sorted into catching media: DMEM/F12 (ThermoFisher) with B27 supplement (ThermoFisher, no Vitamin A, 1:50), N2 supplement (ThermoFisher, 1:100), 15mM HEPES buffer, 0.6% glucose, Penicillin-Streptomycin-Glutamine (Life Technologies, 1:100), and Insulin-Transferrin-Selenium (Life Technologies, 1:1000). Cells were then spun down at 300xg for 5 minutes at 4oC and resuspended in catching media at a concentration of 300 cells/ µL. Cells are then subsequently stained with primary and secondary antibodies as described in the Supplementary Methods. For isolation of T Cells from the brain: For T cell isolation from aged brains, mice were sedated and perfused with 20mL of PBS with heparin sodium salt (Sigma Aldrich, 2mg/mL). Brains were immediately harvested thereafter. The SVZ was isolated as described above for “Single cell RNA-seq using the 10x Genomics Chromium single cell technology”. Tissue dissociation when isolating pure populations of CD8+ T cells was carried out using 2mg/mL collagenase type IV (Gibco) for 30 minutes at 37oC in HBSS with calcium and magnesium (Gibco), containing 14µg/mL of DNAse1 (Sigma Aldrich). The dissociated SVZ was then centrifuged through 22% Percoll (GE Healthcare) in PBS to remove myelin debris. Following centrifugation through Percoll solution, cells were washed with FACS buffer (HBSS, 1% BSA, 1% Glucose). Antibody staining was carried out in FACS buffer at the following dilutions: CD45-PE (Biolegend Cat.# 103105 Clone:30-F11 [1:100]), B220-PeCy5 (Biolegend Cat.# 103209 Clone: RA3-6B2 [1:100]), TER119-PeCy5 (Biolegend Cat.# 116209 Clone:TER-119 [1:100]), CD4-APC (Biolegend Cat.# 100411 Clone:GK1.5 [1:100]), CD8-FITC (Biolegend Cat.# 100705 Clone:53-6.7 [1:100]), CD11b-PerCP/Cy5.5 (Biolegend Cat.#101227 Clone:M1/70 [1:100]), CD3-AF700 (Biolegend Cat.#100216 Clone:17A2 [1:100]). Following primary antibody stain cells were washed with FACS buffer and resuspended in FACS buffer containing 1µg/mL DAPI (ThermoFisher). For isolation of T Cells from the blood or spleen: To isolate CD8+ T Cells from blood. Blood samples were obtained through tail vein snip prior to perfusion. Approximately 50uL of blood was collected into 250uL of a 5U/mL solution of heparin sodium salt (Sigma-Aldrich), in PBS (Corning). Red blood cells were lysed by adding 2mL of ACK lysing buffer (ThermoFisher) for 10 minutes at RT. Following lysis, 10mL of PBS was added to each tube and samples were spun for 10 minutes at 4oC. Samples were stained with an identical antibody panel as described above for isolation of T Cells from the brain.
Instrument	All cell sorting was performed on BD Aria II machines model, and all FACS analysis was was performed on BD LSR II machines housed in the Stanford Shared FACS Facility.
Software	All flow cytometry data was analyzed using FlowJo version 10.2
Cell population abundance	We were able to assess purity in our cell sorts by assessing for the contamination of our cell populations with marker genes for other cell types present in the sub-ventricular zone niche which we were assessing. In single cell RNA-sequencing we observed 100% purity of CD8+ t cells isolated from the brain and 100% purity of neural stem and progenitors, and in bulk sequencing of

BST2+ and BST2- neural stem cells we observed no expression for other markers of contaminating cells. RNA-sequencing was performed on all cell populations isolated by FACS sorting presented in this current study.

Gating strategy

Gating was determined using fluorescent-minus-one controls for each color used in each FACS experiment to ensure that positive populations were solely associated with the antibody for that specific marker.

☒ Tick this box to confirm that a figure exemplifying the gating strategy is provided in the Supplementary Information.